TECHNICAL UNIVERSITY OF CRETE

SCHOOL OF PRODUCTION ENGINEERING AND

MANAGEMENT

CALIBRATION AND VALIDATION OF MACROSCOPIC TRAFFIC FLOW MODELS USING THE INNOVATIVE VALIDATION TOOL CALISTO

Author: Konstantinos Katerinis

Supervisor: Markos Papageorgiou

Chania, 2016

Contents

List of figures

Περίληψη

Τις τελευταίες δεκαετίες, έχουν προταθεί πολλά μαθηματικά μοντέλα κυκλοφοριακής ροής. Τα μοντέλα αυτά μπορούν να χρησιμοποιηθούν κατά το σχεδιασμό νέων ή τη βελτίωση ήδη υπαρχόντων οδικών υποδομών, για την ανάπτυξη και δοκιμή αλγορίθμων πρόβλεψης, για το σχεδιασμό στρατηγικών ελέγχου κυκλοφορίας, καθώς και για πολλές άλλες εφαρμογές. Τα μοντέλα περιλαμβάνουν παραμέτρους των οποίων οι τιμές είναι άγνωστες και μάλιστα μπορεί να διαφέρουν για διαφορετικούς αυτοκινητοδρόμους. Επομένως, πριν από τη χρήση των μοντέλων σε πραγματικές εφαρμογές, είναι απαραίτητη η επικύρωση των μοντέλων χρησιμοποιώντας πραγματικά δεδομένα κυκλοφορίας.

Η διαδικασία της επικύρωσης, αποσκοπεί στον κατάλληλο προσδιορισμό των τιμών των παραμέτρων των μοντέλων έτσι ώστε η αναπαράσταση των κυκλοφοριακών συνθηκών ενός οδικού δικτύου να είναι όσο το δυνατόν ακριβής. Η πιο συνηθισμένη προσέγγιση είναι η ελαχιστοποίηση της απόκλισης μεταξύ των εκτιμήσεων του μοντέλου και των πραγματικών δεδομένων, χρησιμοποιώντας κατάλληλους αλγορίθμους βελτιστοποίησης. Το μη-γραμμικό, μη-κυρτό πρόβλημα εκτίμησης των παραμέτρων είναι γνωστό ότι έχει πολλά τοπικά ελάχιστα και ως εκ τούτου είναι κατάλληλο να χρησιμοποιούνται μόνο αλγόριθμοι που δεν κάνουν χρήση παραγώγων.

Στη βιβλιογραφία υπάρχει περιορισμένος αριθμός εργασιών που πραγματοποιούν επικύρωση μακροσκοπικών μοντέλων κυκλοφοριακής ροής είτε λόγω του γεγονότος ότι είναι σχετικά δύσκολο να αποκτήσει κάποιος πρόσβαση σε πραγματικά δεδομένα κυκλοφορίας, είτε επειδή δεν είναι διαθέσιμο, έως τώρα, κάποιο εργαλείο που να μπορεί εύκολα να χρησιμοποιηθεί για να επιλύσει το πρόβλημα εκτίμησης των παραμέτρων. Σε αυτή την εργασία ένα καινοτόμο λογισμικό-εργαλείο έχει αναπτυχθεί για την επικύρωση μακροσκοπικών μοντέλων κυκλοφοριακής ροής με μία εύχρηστη διεπιφάνεια εργασίας.

Το εργαλείο αυτό χρησιμοποιήθηκε για την σύγκριση διαφόρων μοντέλων κυκλοφοριακής ροής κάνοντας χρήση πραγματικών δεδομένων από έναν αυτοκινητόδρομο στο Ηνωμένο Βασίλειο. Συγκεκριμένα εξετάστηκαν τέσσερις εκδοχές ενός μακροσκοπικού μοντέλου πρώτης τάξης καθώς και ένα μακροσκοπικό

μοντέλο δεύτερης τάξης, για λόγους σύγκρισης. Τα αποτελέσματα που λάβαμε ήταν ικανοποιητικά για όλα τα μοντέλα και ιδιαίτερα κάποια από αυτά αναπαριστούν τις συνθήκες κυκλοφορίας με μεγαλύτερη ακρίβεια. Τα εξεταζόμενα μοντέλα αξιολογήθηκαν συγκριτικά κάνοντας χρήση πραγματικών δεδομένων από διαφορετικές ημέρες από τον ίδιο αυτοκινητόδρομο.

1 Introduction

This chapter includes first, in Section 1.1, a short introduction on the traffic flow models, then, in Section 1.2, there is the description of the problem under study and the approach followed within the thesis and finally the outline of the thesis is given in Section 1.3.

1.1 Traffic flow models

During the last decades, several mathematical models to describe the road traffic flow have been proposed (Hoogendoorn and Bovy, 2001). The traffic flow models can be utilized for the planning of new road infrastructures or for the modification of existing ones; they are also utilized for the development and testing of traffic flow estimation algorithms, traffic control strategies and other operational tools. The traffic flow models include a set of parameters and their values may vary for different road networks. Depending on the level of detail they use, the models are classified as macroscopic or microscopic. The macroscopic traffic flow models usually include lower number of parameters compared to microscopic models; also, they have an analytical form, which allows their usage for various significant traffic engineering tasks (e.g traffic estimation, control strategy design etc.) beyond simulation. The macroscopic traffic flow models are classified as first-, second- or higher-order models, depending on the number of differential equations they include. First-order models are known for their simplicity and computational efficiency and for this reason have been widely used in the past. However, these models fail to capture some real traffic phenomena such as the stop-and-go waves and the capacity drop phenomenon. Furthermore they don't consider factors such as the drivers' reaction time and the vehicles acceleration capabilities. On the other hand, second or higher-order models include extra equations to describe the dynamics of speed. As a result they are able to reproduce the traffic phenomena mentioned above, however they are characterized by higher complexity, higher number of parameters, and higher computation effort, which makes their use difficult in optimization problems built upon them.

1.2 Objectives and approach

Given the simplicity of first-order models, this thesis examines and compares different formulations of a popular first-order model, namely the LWR model. Moreover a second-order model (METANET) is included for comparison purposes. The models are applied to a real traffic network in the UK using real traffic data. In order to compare the examined models they are first calibrated, for this particular network, i.e. the optimal parameter values are estimated using real traffic data. The calibration and validation of the models is performed using the innovative software tool CALISTO (Spiliopoulou et al., 2014) which has been recently developed and makes the calibration and validation of macroscopic traffic flow models an easy task.

1.3 Thesis outline

The diploma thesis is organized as follows. Chapter 2 presents the traffic flow models that are examined in this thesis and the unknown parameters they include whose values need to be estimated. In Chapter 3, the model calibration procedure is described first, then the software tool CALISTO used for the calibration and validation of the selected traffic flow models is presented, followed by the description of the Nelder-Mead optimization algorithm which is employed to solve the parameter estimation problem. Chapter 4, includes information about the freeway site examined in this particular thesis and the real traffic data used for the calibration and validation of the models. Furthermore, Chapter 4, contains the calibration and validation for all utilized models as well as the comparison of the examined models. Finally, Chapter 5 summarizes the main conclusions and remarks of this thesis.

2 Macroscopic traffic flow models

This chapter presents the macroscopic traffic flow models that are used in this thesis. Section 2.1 includes a brief introduction on the traffic flow models and their classification. Furthermore, in Section 2.2 various formulations of a first-order model are presented and finally in Section 2.3 the METANET model is discussed.

2.1 Classification of traffic flow models

Over the last decades a high number of traffic flow models has been developed and applied for different traffic engineering tasks. Traffic flow models may be classified based on the level of detail with which the vehicular flow is described. In particular, there are three main classes:

1. **Microscopic models** (high level of detail)
2. **Mesoscopic models** (medium level of detail)
3. **Macroscopic models** (low level of detail)

Microscopic models describe the space-time behavior of individual vehicles and their interactions with the surrounding traffic. This behavior is described by dynamic variables such as position, speed and acceleration. Microscopic models require high computing power, but they provide accurate simulation of the traffic flow.

Mesoscopic models describe the traffic flow at a medium level of detail. In particular, the models do not distinguish or trace the individual behavior of vehicles but they represent the behaviour of small traffic groups, the activities and interactions of which are described at a low detail level.

Macroscopic models describe traffic in an aggregate manner considering traffic flow as a compressible fluid with specific characteristics. The traffic variables used to describe the dynamics of this fluid are the mean speed, the density and the traffic flow (or volume). The macroscopic traffic flow models are classified as first-, second- or higher-order models, depending on the number of differential equations they include. In this thesis several first-order models and a second-order model are applied and compared using real traffic data from a freeway stretch in the UK. The employed models are described in the following sections.
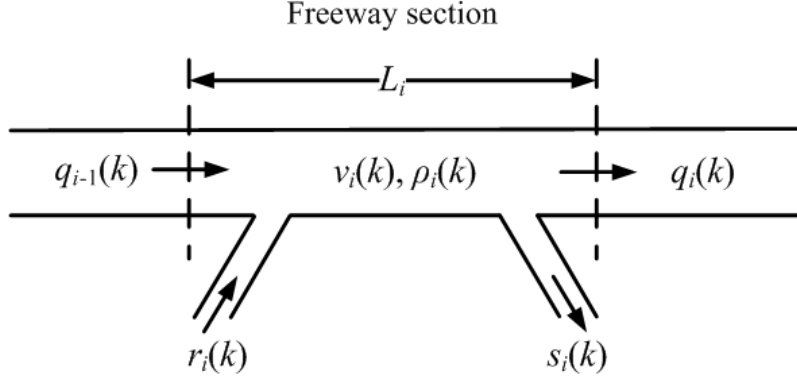
Figure 1 Freeway discretization.

2.2 Various first-order model formulations

Four first-order models are examined within this thesis. All four models are discretized versions of the LWR (Lighthill and Whitham, 1955; Richards, 1956) first-order model. The models consider that the freeway stretch is discretized into consecutively numbered sections i, with respective length L_i, and number of lanes λ_i (see Figure 1). Time is also discretized into uniform intervals of duration T, with a discrete time index $k = 0,1,\ldots,K$. The state variable for section i is the density $\rho_i(k)$, which corresponds to the number of vehicles included in section i at the time instant kT, and is calculated as follows:

$$\rho_i(k+1) = \rho_i(k) + \frac{T}{L_i \lambda_i}[q_{i-1}(k) - q_i(k) - s_i(k) + r_i(k)]. \qquad (1)$$

This is a conservation-of-vehicles equation, where $q_i(k)$ is the traffic flow exiting section i and entering section $i + 1$, $r_i(k)$ is the traffic flow entering the freeway section i from an on-ramp and $s_i(k)$ is the traffic flow exiting the freeway section from an off-ramp, and equals to $s_i(k) = \beta_i(k)q_i(k)/[1 - \beta_i(k)]$ where $\beta_i(k)$ is the splitting ratio. The flow $q_i(k)$ exiting each section i is estimated as the minimum of two quantities:

$$q_i(k) = \min\{D_i(k), S_{i+1}(k)\} \qquad (2)$$

where $D_i(k)$ is the maximum flow that can be supplied by section i, during the time interval k and $S_{i+1}(k)$ is the maximum flow that can be received by section $i+1$ over the same time interval. The functions $D_i(k)$ and $S_{i+1}(k)$ are calculated as follows:

$$D_i(k) = min\{Q_{cap,i}, g_i(\rho_i(k))\}(1 - \beta_i(k)) \tag{3}$$

$$S_{i+1}(k) = min\{Q_{cap,i+1}, w_{i+1}(\rho_{max,i+1} - \rho_{i+1}(k))\lambda_{i+1}\} - r_{i+1}(k) \tag{4}$$

where $Q_{cap,i}$ and $Q_{cap,i+1}$ are the flow capacities of sections i and $i+1$, respectively; $\rho_{max,i+1}$ is the maximum density of section $i+1$; w_{i+1} is the congestion wave speed of section $i+1$; and $g_i(\rho_i(k))$ is a function that depends on the density of section i.

The utilized demand and supply functions, $D_i(k)$ and $S_i(k)$ respectively, define the static relation between the flow $q_i(k)$ and density $\rho_i(k)$ of section i, also known as the fundamental diagram (FD). In this study, different formulations of the fundamental diagram are utilized resulting to different first-order models. More specifically, the supply function $S_i(k)$ is assumed to be linear (with a negative slope w_i), while the demand function $D_i(k)$ includes a non-decreasing function $g_i(\rho_i(k))$. Different shapes of the function g_i are examined and compared.

In particular, if a triangular-shaped FD is considered (see for example Figure 2(a)) the CTM model (Daganzo, 1995, 1994)) is obtained. In this case, $g_i(\rho_i) = v_{f,i}\rho_i(k)\lambda_i$, $g_i(\rho_{cr,i}) = Q_{cap,i}$ and $w_i = Q_{cap,i}/(\rho_{max,i} - \rho_{cr,i})\lambda_i$. This formulation has two main drawbacks: first, when using realistic free flow and congestion wave speeds, it leads to high and sometimes unrealistic capacity flow; second, only one speed value is considered for all under critical densities which is often not compatible with traffic observations. To overcome the first issue, a trapezoidal FD can be used (see for example Figure 2(b)) where $g_i(\rho_i) = v_{f,i}\rho_i(k)\lambda_i$, $g_i(\rho_{cr,i}) \geq Q_{cap,i}$ and $w_i \geq Q_{cap,i}/(\rho_{max,i} - \rho_{cr,i})\lambda_i$. In this case the critical density, instead of being a fixed

point for both the FD parts, can be selected within an interval of densities, increasing the degree of freedom for model calibration. Nevertheless, in real traffic the observed speed may be characterized by a decreasing-slope behavior also for low densities, which can be reflected by using a nonlinear concave function $g_i(\rho_i)$ (see Figure 2(d)), where $g_i(\rho_{cr,i}) = Q_{cap,i}$ and $w_i = Q_{cap,i}/(\rho_{max,i} - \rho_{cr,i})\lambda_i$. As an example, a nonlinear exponential function can be employed as proposed in (Papageorgiou and Messmer, 1990). The use of such a function allows for mean speed variations for undercritical densities, thus may produce more realistic results. A similar behavior can also be obtained, without much loss of accuracy considering a piecewise linear approximation (see Figure 2(c)) of the nonlinear function which is helpful in case linear constraints are needed for the formulation of an optimization problem.

Finally the mean speed $v_i(k)$ at every section i, is computed, using the fundamental relation $v_i(k) = q_i(k)/\rho_i(k)\lambda_i$.

2.3 METANET

The METANET model (Messmer, Papageorgiou 1990) is a discretized and enhanced variation of the second order model of Payne (Payne, 1971). In particular, the model considers that the freeway is discretized into consecutively numbered sections i, with respective length L_i, and number of lanes λ_i. Time is also discretized into uniform intervals of duration T. For each discrete time $k = 0,1, \dots, K$, the model calculates at each section i, the density $\rho_i(k)$, the flow $q_i(k)$ and the mean speed $v_i(k)$ according to the following equations:

$$\rho_i(k + 1) = \rho_i(k) + \frac{T}{L_i\lambda_i}[q_{i-1}(k) - q_i(k) - s_i(k) + r_i(k)] \qquad (5)$$

$$q_i(k) = v_i(k)\rho_i(k)\lambda_i \qquad (6)$$
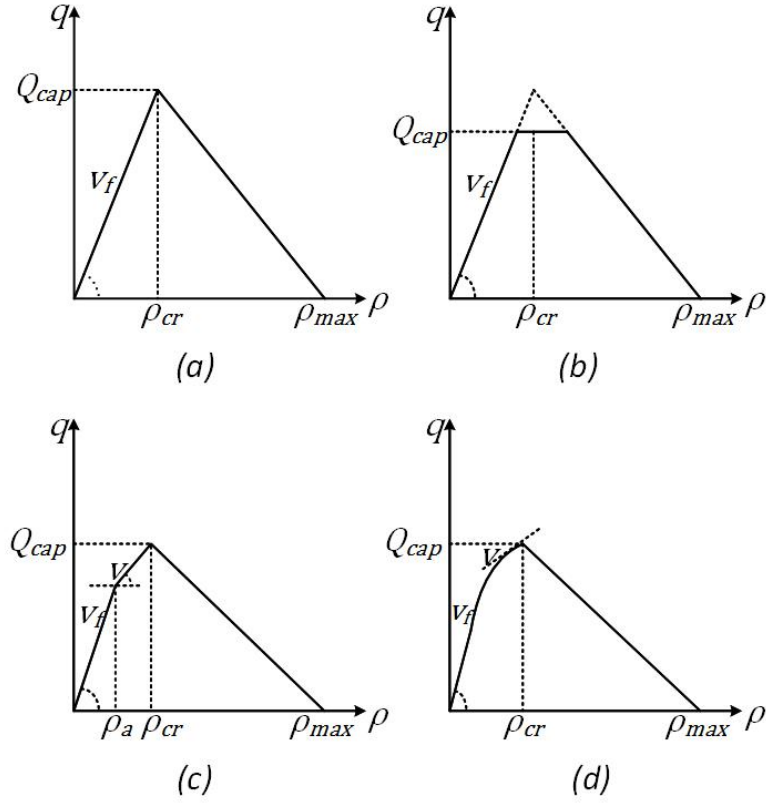
Figure 2 Different choices for the left-hand side of the fundamental diagram corresponding to: (a) a triangular FD (CTM), (b) a trapezoidal FD, (c) a piecewise linear FD and (d) a nonlinear FD.

$$v_i(k+1) = v_i(k) + \frac{T}{L_i} v_i(k)[v_{i-1}(k) - v_i(k)] \qquad (7)$$

$$+ \frac{T}{\tau}\left[V^e\big(\rho_i(k)\big) - v_i(k)\right] - \frac{\nu T[\rho_{i+1}(k) - \rho_i(k)]}{\tau L_i[\rho_i(k) + \kappa]}$$

where τ (a time constant), ν (an anticipation constant) and κ are model parameters. The function $V^e\big(\rho_i(k)\big)$ corresponds to the fundamental diagram and is calculated as follows:

$$V^e\big(\rho_i(k)\big) = v_{f,i}\,exp\left[-\frac{1}{\alpha_i}\left(\frac{\rho_i(k)}{\rho_{cr,i}}\right)^{\alpha_i}\right] \qquad (8)$$

16

where $v_{f,i}$ is the free flow speed, $\rho_{cr,i}$ is the critical density (for which the flow at section i is maximized) and α_i is a further model parameter for section i. Moreover, the mean speed calculated by the model should not be lower than a minimum value v_{min}. In (Papageorgiou et al., 1990) two additional terms were proposed for more accurate modeling of merging and lane drop phenomena. In particular, the impact on mainstream speed due to an on-ramp merging flow is considered by adding the term $-\delta T\, r_i(k)\, /\, L_i\lambda_i(\rho_i(k) + \kappa)$ into (7) for the merging section, where δ is a model parameter and $r_i(k)$ is the inflow from the on ramp. In order to take into account the impact on speed due to intensive lane-changing at lane-drop areas, the term $-\varphi T \Delta\lambda\rho_i(k)v_i(k)^2/L_i\lambda_i\rho_{cr,i}(k)$, is added to (7) for the section immediately upstream of the lane drop, where φ is a model parameter and $\Delta\lambda$ is the number of dropped lanes.

3 Traffic flow model calibration

As presented in the previous chapter, the traffic flow models include a set of parameters, whose values may differ for different freeway sites. In order to specify the unknown model parameter values, for a particular freeway site, the models should be first calibrated against real traffic data. In the following, Section 3.1 describes the model calibration procedure, Section 3.2 presents the software tool CALISTO that will be employed in order to calibrate the investigated traffic flow models and Section 3.3 shortly describes the optimization algorithm that will be utilized to solve the parameter estimation problem.

3.1 Model calibration procedure

The model parameter calibration aims at enabling a macroscopic traffic flow model to represent the traffic conditions of a freeway network with the highest achievable accuracy. The estimation of the unknown model parameters is not an easy task, since the system equations are highly nonlinear in both the parameters and the state variables.

Consider that a macroscopic discrete-time state-space model is described by the following state equation,

$$\mathbf{x}(k + 1) = f[\mathbf{x}(k), \mathbf{d}(k), \mathbf{p}], \qquad k = 0, 1, \dots, K - 1$$
$$\mathbf{x}(0) = \mathbf{x}_0$$

(9)

where k is the discrete time index; $\mathbf{x}$ is the state vector, $\mathbf{d}$ is the external variable (disturbance) vector and $\mathbf{p}$ is the model parameter vector. In particular, the state vector $\mathbf{x}$ includes the section densities in the case of all four first order formulations and in the case of METANET model the section densities and mean speeds. The external variable vector $\mathbf{d}$ consists of all known boundary conditions such as the network inflows, the turning rates at bifurcations, and the network downstream densities. The model parameter vector $\mathbf{p}$ includes the unknown model parameters that need to be specified for each model.

If the initial state $\mathbf{x}_0$ is given and the external variables $\mathbf{d}(k)$ are known over a time horizon $k = 0, \dots, K-1$, then the parameter estimation problem can be formulated as a nonlinear least-squares output error problem which aims at the minimization of the discrepancy between the model calculations and the real traffic data by use of the following cost function

$$J(\mathbf{p}) = \sqrt{\frac{1}{K} \sum_{k=0}^{K-1} [\mathbf{y}(k) - \mathbf{y}^m(k)]^2} \tag{10}$$

subject to (9); where $\mathbf{y}(k) = \mathbf{g}[\mathbf{x}(k)]$ is the measurable model output vector (typically consisting of flows and mean speeds at various locations of the network) and $\mathbf{y}^m(k)$ is the real measured traffic data (consisting of flows and speeds at the corresponding network locations). The model parameters are selected from a closed admissible region of the parameter space, which may be defined on the basis of physical considerations. The determination of the optimal parameter set must be performed by means of a suitable nonlinear programming routine, whereby for each choice of a new parameter vector $\mathbf{p}$, the value of the performance index (PI) (10) may be computed by a simulation run of the model equations shown in Figure 3.

After the calibration procedure, the resulting traffic flow models must be validated before their use in a real implementation. The validation procedure ensures that the resulting model reflects reliably the traffic characteristics of the specific network, thus it may reproduce its typical traffic conditions. To this end, the model is applied to the same freeway, albeit using different data for the disturbance vector $\mathbf{d}$ and initial state $\mathbf{x}_0$, than the ones used for its calibration and the model output $\mathbf{y}$ is compared to the corresponding real traffic data $\mathbf{y}^m$. In other words, the calibration procedure uses real traffic data from a specific date, while for the validation procedure data from different dates are being used.

The calibration and validation of the selected traffic flow models is performed by use of the innovative software tool CALISTO, which is described in the following section.
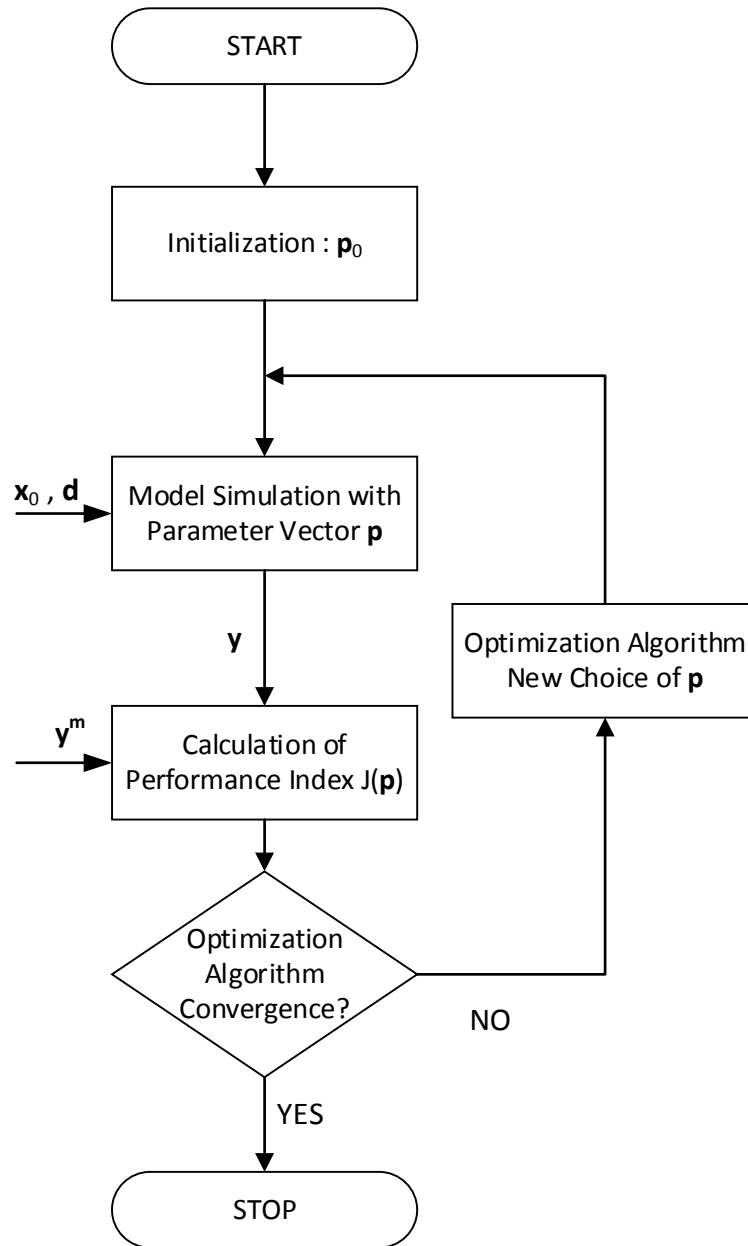
Figure 3 Model calibration procedure.

3.2 CALISTO software tool

CALISTO (CALIbrationS Tool) (Spiliopoulou et al., 2014) is an innovative software tool which enables the calibration and validation of macroscopic traffic flow models for various freeway sites using real traffic data. For the purposes of this thesis the examined traffic flow models, presented in Chapter 2 have been programmed and
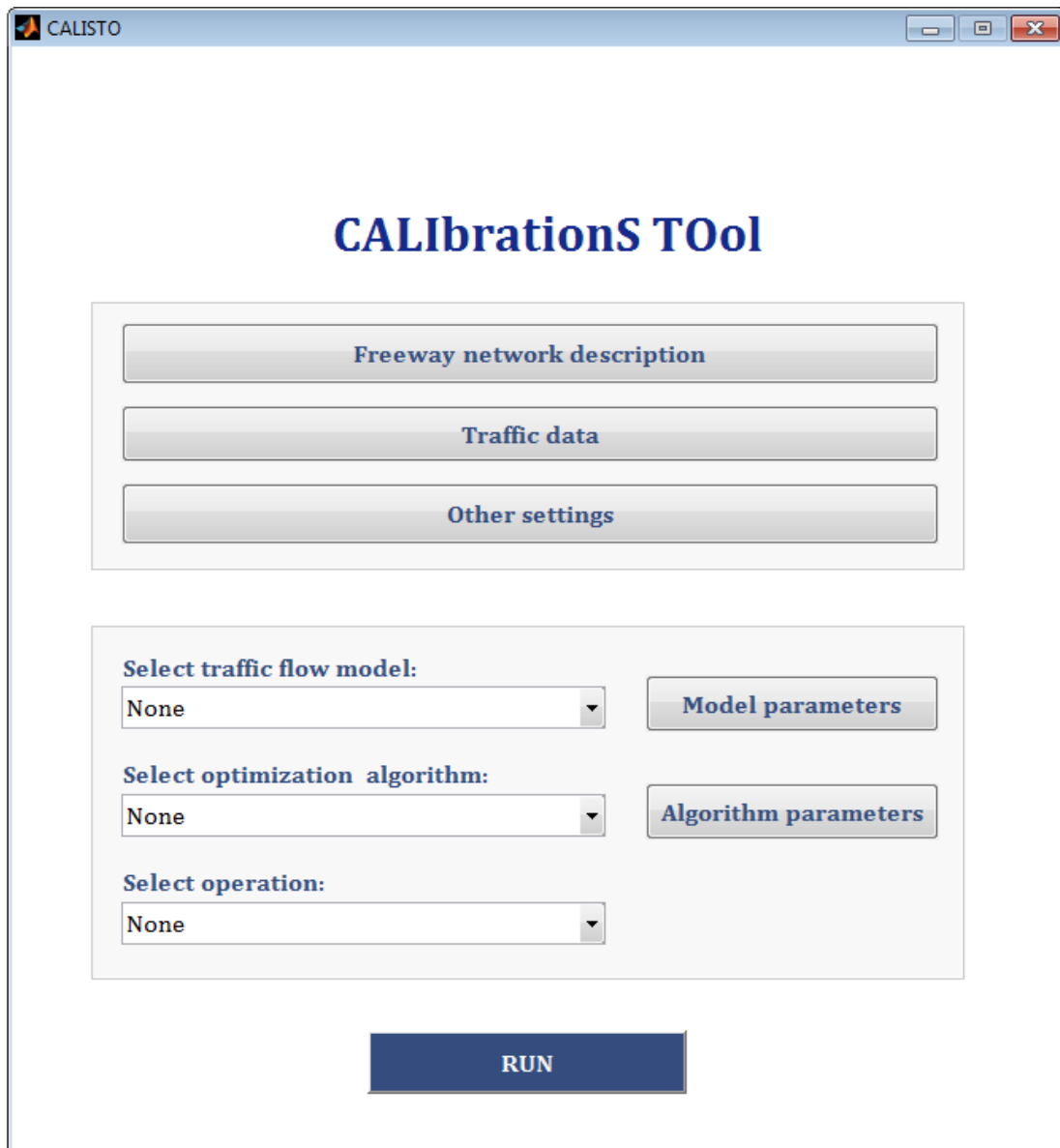
Figure 4 CALISTO application window.

introduced into CALISTO software. This section briefly describes the software tool. In the following, Section 3.2.1 presents the application window of the software, Section 3.2.2 describes the software tool input data and Section 3.2.3 presents the software tool output results.

3.2.1 CALISTO application window

Figure 4 presents the application windows of the software which contains the following basic elements:

- **Freeway network description:** this feature includes all the required information to describe the freeway site under investigation.
- **Traffic data:** consists of information for the simulated traffic data, such as the measurement step, the duration of the simulation and the location of the input file that contains the real traffic data.
- **Other settings:** contains the simulation step and some extra features concerning the utilized performance index and the simulation outputs.
- **Selection of the traffic flow model:** one of the available traffic flow models can be selected and its corresponding model parameter values should be specified.
- **Selection of the optimization algorithm:** one of the available optimization methods can be employed to perform the calibration of the chosen traffic flow model.
- **Selection of the operation:** two operations are available, Calibration or Validation.
- **Execution (Run):** the selected operation is executed taking into account all the introduced information.

These elements are presented in detail in the following sections.

3.2.2 Network and traffic data description

The first two buttons on the application window (Freeway network description, Traffic data) contain information related to the investigated network and the utilized real traffic data.

The **Freeway network description** button opens an editor which includes all the required information so that a freeway network is described in detail. In particular, the user must insert the number of mainstream freeway links, the length and the number of lanes of every link, the number of on-ramps and off-ramps and their location, the number of detector stations and their location etc. Figure 5 shows the *Freeway network description* editor which contains the information given to describe the network considered within this thesis.

The **Traffic data** button opens an editor which contains all the required information related to the utilized real traffic data. In particular, the user must define the simulation duration, the measurement step of the real traffic data, as well as, the location of the traffic data input file. Figure 6 shows the *Traffic data* editor which includes the information used for the simulated traffic data within this thesis.
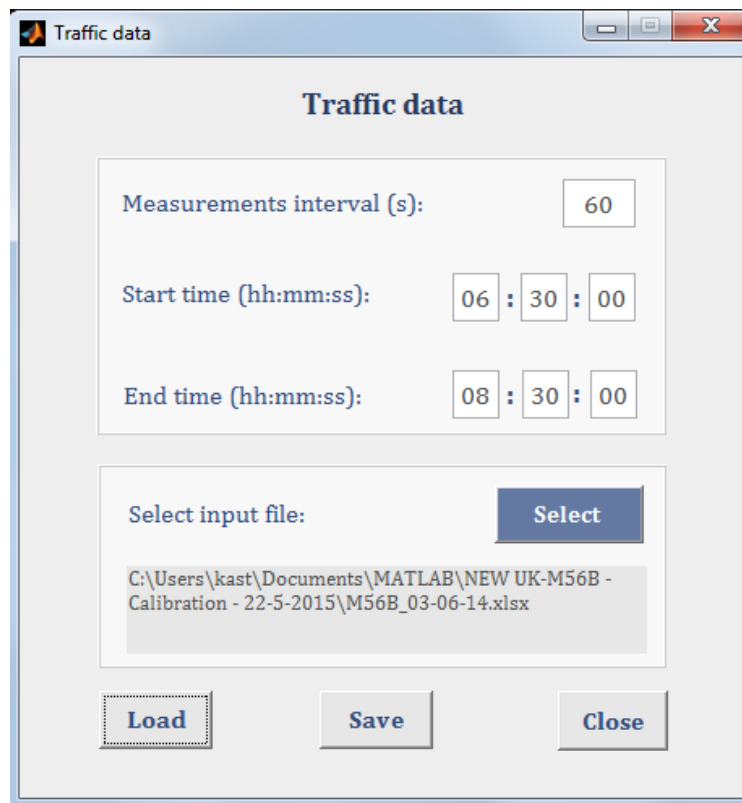
Figure 5 Freeway network description editor.

3.2.3 Calibration/validation set-up

The third button on the application window, named **Other settings**, opens an editor which includes some features related to the simulation set-up, such as the simulation step of the employed traffic flow model. Moreover, it contains the flow and speed error weights included in the calculation of the performance index. In particular, the utilized (within the software) performance index is given by the following equation:

Figure 6 Traffic data editor.

Figure 7 Other settings editor.

$$PI = w_f \cdot RMSE_{flows} + w_s \cdot RMSE_{speeds}$$

where $RMSE_{flows}$ and $RMSE_{speeds}$ are the root mean squared errors of the real flow and speed measurements and the corresponding model estimations, respectively, and w_f and w_s are the corresponding error weights. Finally, the editor includes some choices regarding the simulation output plots. Figure 7 illustrates the *Other settings* editor which presents the information used within this thesis.

The next step for the user is to choose one of the available macroscopic traffic flow models included in the software. Figure 7 depicts the list of the available traffic flow models within the current version of the software. In particular, it includes four discretized first-order models as well as the second order model METANET. See Chapter 2 for a description of the models.

After the selection of the macroscopic model the user must choose one of the available optimization algorithms to perform the model calibration. Ther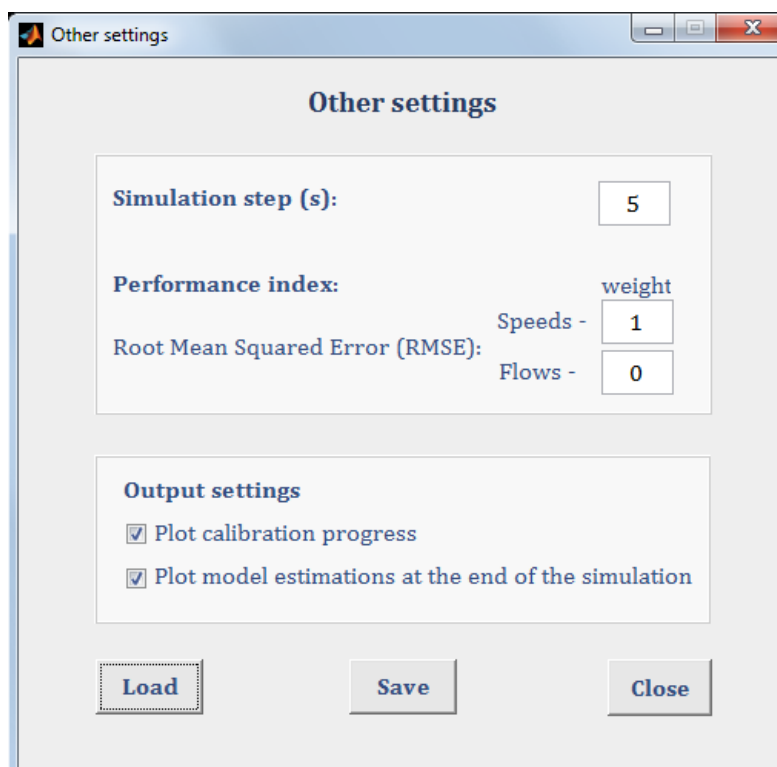e are three available optimization methods in the current version of the software. In particular, the Nelder-Mead algorithm, a Genetic algorithm and the Cross-entropy method. Note that all three algorithms are derivate-free algorithms. The optimization method used within this thesis is the Nelder-Mead optimization method. See Section 3.3 for a detailed description of the Nelder-Mead algorithm.

Finally, the software offers to the user the option to select between two operations, i.e. calibration or validation (see Figure 10). See Section 3.1 for a description of the model calibration and validation procedure.

3.2.4 Calibration/validation results

In order to perform the calibration or validation of the selected model the user should click on the *Run* button (see Figure 10). If the selected operation is *Calibration* then the following results are obtained:

— Graph of the calibration progress over iterations as shown in Figure 11. This graph appears only if this is selected by the user (see Figure 7).

— A window including the optimal model parameter values (as shown in Figure 12).
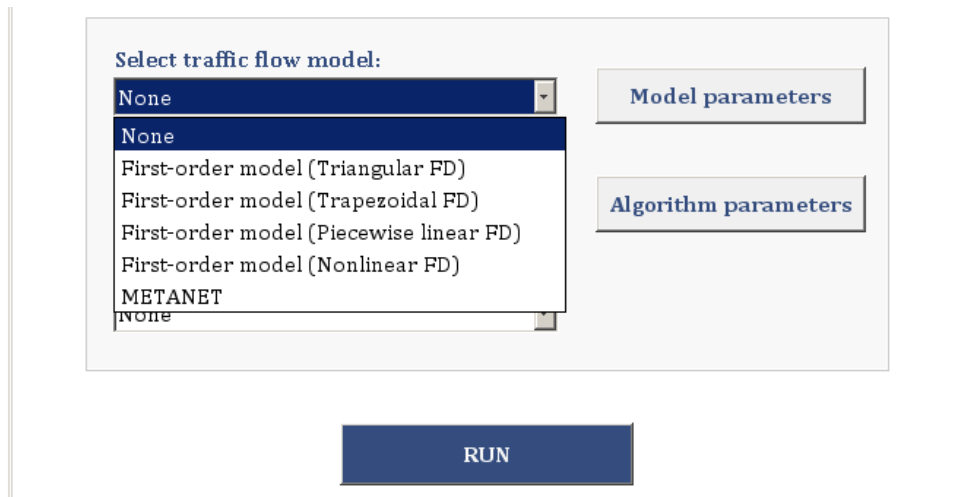
Figure 8 List of the available traffic flow models within CALISTO software.
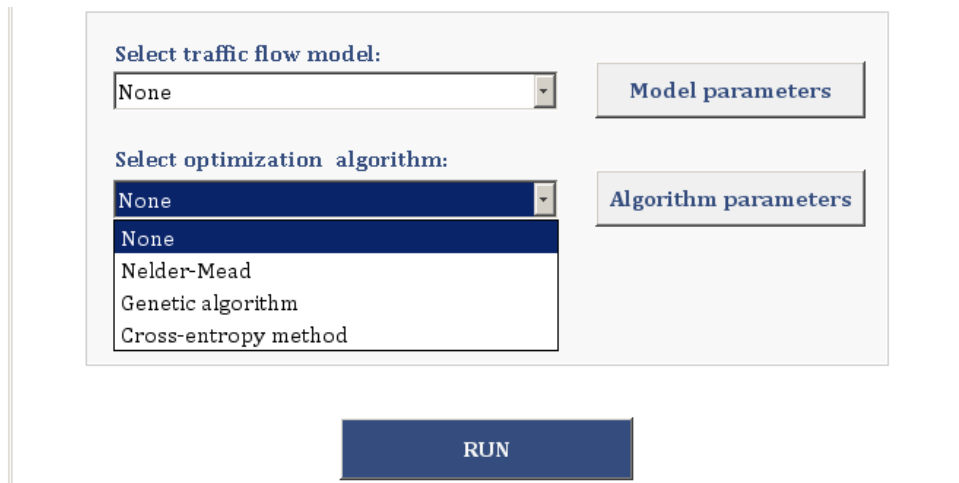
Figure 9 List of the available optimization algorithms within CALISTO software.
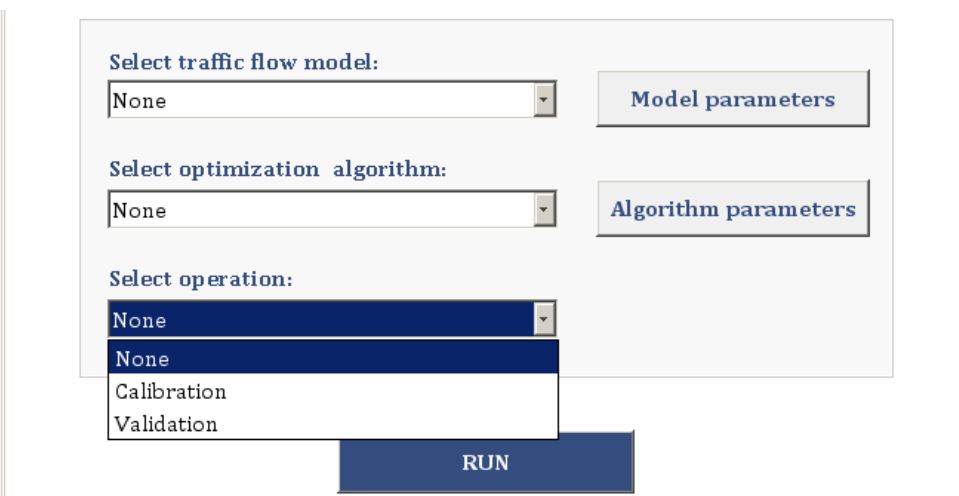
Figure 10 List of the available operations available within CALISTO software.
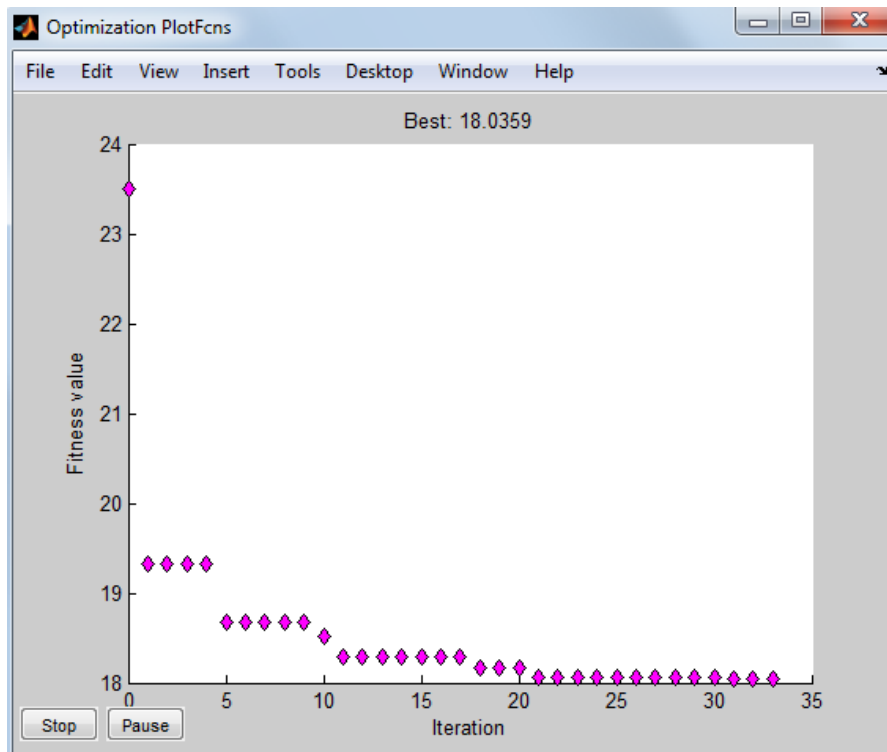
Figure 11 Plotted calibration process.

— Time plots of the real traffic measurements (flows, speeds and densities) and the corresponding model estimations for all detector locations (see for example Figure 13). These plots appear only if this is selected by the user (see Figure 7).

— Output files including all the information related to the calibration results (e.g. optimal parameter values, flow, speed and density estimations at all network segments, performance index value etc).

If the selected operation is *Validation* then the following results are obtained:

— Time plots of the real traffic measurements (flows, speeds and densities) and the corresponding model estimations for all detector locations (see again Figure 10).

— Output files including all the information related to the validation results (e.g. flow, speed and density estimations at all network segments, performance index value etc).

Figure 12 Estimated model parameter values.
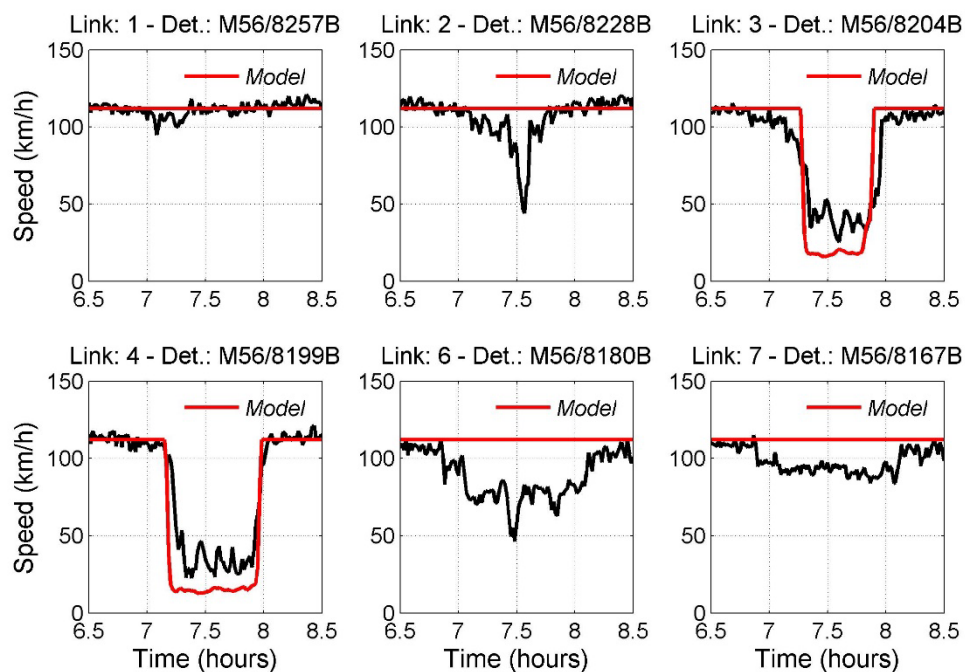
Figure 13 Time series of the real speed measurements and the model's estimation of speed.

3.3 Nelder-Mead algorithm

In this thesis the Nelder-Mead algorithm (Lagarias et al., 1998) is employed to solve the model parameter estimation problem. Nelder-Mead is one of the best known algorithms for multidimensional unconstrained optimization. The method does not require any derivative information, which makes it suitable for problems with nonlinear, discontinuous or stochastic cost function.

The method uses a simplex (see Figure 14), i.e. a n-dimensional geometrical shape with $n + 1$ vertices. Every vertex $\mathbf{p}_i$, where $i = 1, \dots, n + 1$, corresponds to a potential solution which in turn corresponds to a cost function value, $J(\mathbf{p}_i)$. The method starts with an initial working simplex and then performs a sequence of transformations of the working simplex, aiming to decrease the cost function value at its vertices. In particular, one iteration of the Nelder-Mead method consists of the following three steps.

1. **Ordering:** The algorithm orders the vertices of the working simplex with respect to the corresponding cost function values, to satisfy $J(\mathbf{p}_1) \leq J(\mathbf{p}_2) \leq \cdots \leq J(\mathbf{p}_{n+1})$.

2. **Centroid:** The centroid $\mathbf{p}_c$ of all the vertices is calculated excluding the worst vertex $\mathbf{p}_{n+1}$.
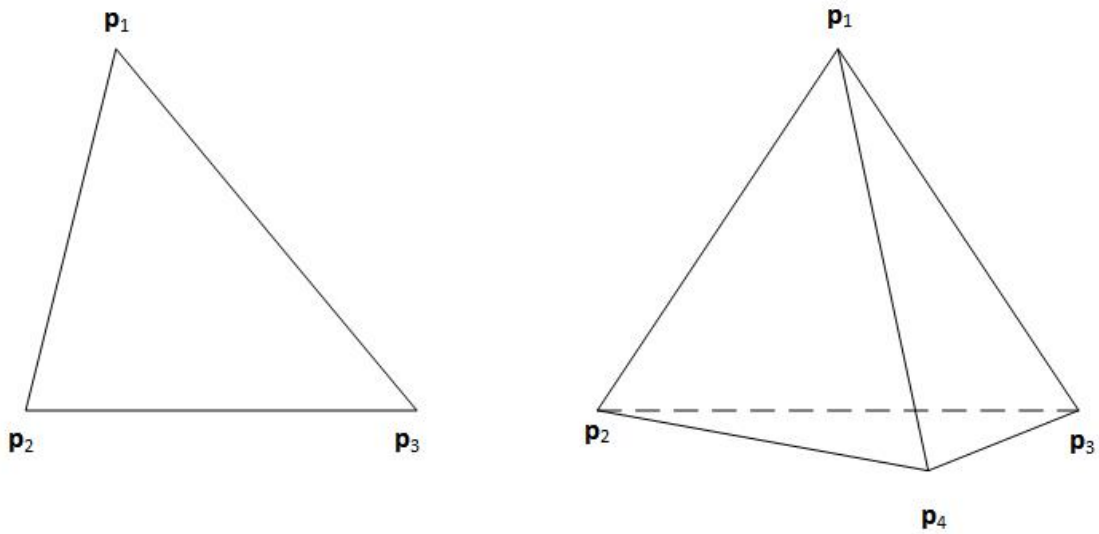
Figure 14 Example of a simplex in $\mathbb{R}_2$ (triangle), and a simplex in $\mathbb{R}_3$(tetrahedron).

$$\mathbf{p_c} := \frac{1}{n} \sum_{i \neq n+1} \mathbf{p}_i$$

3. **Transformation:** The new working simplex is computed from the current one. At first the algorithm tries to replace only the worst vertex $\mathbf{p}_{n+1}$ with a better point by using reflection, expansion or contraction. If this succeeds, then the accepted point becomes the new vertex of the working simplex. If this fails, the algorithm shrinks the simplex towards the best vertex $\mathbf{p_1}$. In this case, n new vertices are computed.

In the following, the working simplex transformations are described in detail.

- **Reflection:** The algorithm computes the reflected point $\mathbf{p}_r = \mathbf{p}_c + \zeta(\mathbf{p}_c - \mathbf{p}_{n+1})$. If the reflected point is better than the second worst, but not better than the best i.e.: $J(\mathbf{p}_1) < J(\mathbf{p}_r) < J(\mathbf{p}_n)$ then the new working simplex is obtained by replacing the worst point $\mathbf{p}_{n+1}$ with the reflected point $\mathbf{p}_r$ and the algorithm returns to the first step.

- **Expansion:** If the reflected point is the best point computed so far, i.e.: $J(\mathbf{p}_r) < J(\mathbf{p}_1)$, then the method computes the expanded point $\mathbf{p}_e = \mathbf{p}_c + \chi(\mathbf{p}_c - \mathbf{p}_{n+1})$. If the expanded point is better than the reflected point, $J(\mathbf{p}_e) < J(\mathbf{p}_r)$, then the new working simplex is obtained by replacing the worst point $\mathbf{p}_{n+1}$ with the expanded point $\mathbf{p}_e$ and the algorithm returns to the first step. Otherwise the new working simplex is obtained by replacing the worst point $\mathbf{p}_{n+1}$ with the reflected point $\mathbf{p}_r$ and the algorithm goes to the first step.

- **Contraction:** If $J(\mathbf{p}_r) \geq J(\mathbf{p}_n)$, the contraction point $\mathbf{p}_{contr}$ is computed as $\mathbf{p}_{contr} = \mathbf{p}_c + \gamma(\mathbf{p}_c - \mathbf{p}_{n+1})$. If $J(\mathbf{p}_{contr}) < J(\mathbf{p}_{n+1})$ then the new working simplex is obtained by replacing the worst point $\mathbf{p}_{n+1}$ with the contracted point $\mathbf{p}_{contr}$ and the algorithm returns to the first step. Otherwise, the algorithm performs a shrink transformation.

- **Shrink:** The algorithm replaces all points, except for the best, using the equation $\mathbf{p}_i = \mathbf{p}_1 + \sigma(\mathbf{p}_i - \mathbf{p}_1)$ for all $i \in \{2, \dots, n+1\}$. Then the algorithm returns to step 1.

The simplex transformations in the Nelder-Mead are controlled by four parameters: ζ for *reflection*, χ for *contraction*, γ for *expansion* and σ for *shrinkage*. Typical values for these parameters used in most implementations are

$$\zeta = 1, \qquad \chi = \frac{1}{2}, \qquad \gamma = 2, \qquad \sigma = \frac{1}{2}.$$

The procedure described above continues until the working simplex becomes sufficiently small or when the values $J(\mathbf{p}_i)$ are close enough to each other.

The Nelder-Mead method typically requires only *one* or *two* function evaluations per iteration, except in shrink transformations, which are extremely rare in practice. This is very important in applications where each function evaluation is very expensive or time-consuming. For such problems, the method is often *faster* than other methods, especially those that require at least n function evaluations per iteration. On the other hand, in some cases the method may perform a large number of iterations without significant improvement of the cost function value. To cope with this problem, restarting the algorithm several times, with reasonably small number of allowed iterations per each run may be a heuristic solution. Moreover, the evolution of the working simplex and the produced best solution are dependent on the initial working simplex, since the algorithm searches for the new points using the vertices of the working simplex. To face this fact, multiple algorithm runs should be carried out using different initial vertices for the working simplex.

4 Calibration and Validation results

This chapter includes the calibration and validation results of various macroscopic first-order traffic flow models, which are based on the same simple first-order model but they use different formulation of the fundamental diagram. Moreover, a second-order model is included for comparison purposes. In the following, Section 4.1 describes the examined freeway site and the real traffic data used in the presented investigations. Section 4.2 includes the calibration and validation results for all examined models obtained by use of the innovative tool CALISTO. Finally, Section 4.3 summarizes the obtained results and compares the investigated models.

4.1 Freeway site and real traffic data

The freeway stretch considered for the present investigations is a part of the M56 motorway in the United Kingdom, direction from Chester to Manchester. The considered 3-lane freeway stretch is 9.45 km long and includes one off-ramp and a two-lane on-ramp, which, before reaching the motorway, is divided into two separate lanes which enter the freeway at two different locations, as shown in Figure 15. In order to model the network by use of the examined traffic flow models, the freeway stretch is divided into 7 links and each freeway link is subdivided in model cells (or segments) of equal length (about 250 m each). Note that the model equations (presented in Chapter 2) are directly applicable to the motorway cells. Figure 15 displays the length of each link, the location of the on-ramps and off-ramp, as well as the locations of the detectors stations.
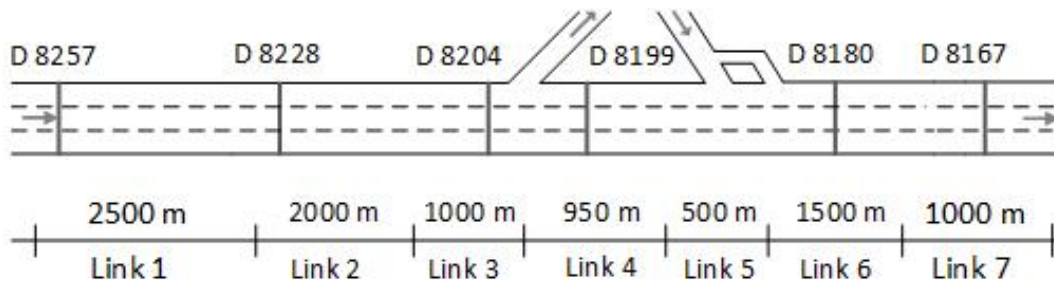

Figure 15 Representation of the considered freeway stretch.
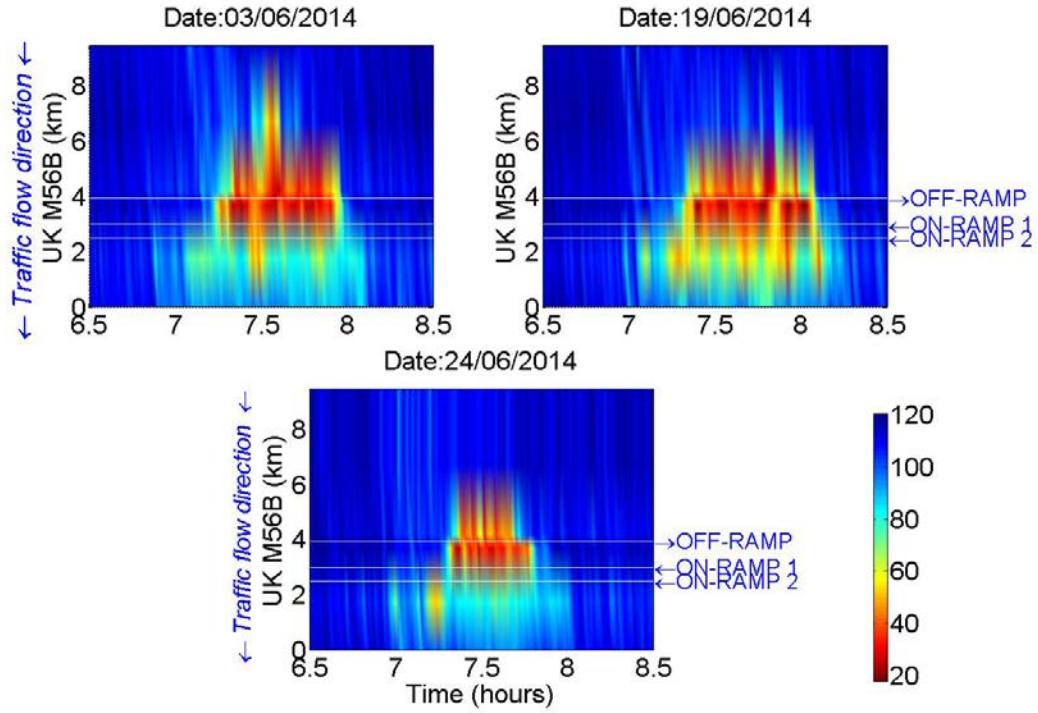
Figure 16 Time-space diagram of the real measured speed at the considered freeway for three different days.

The traffic data used in the current investigations are obtained from the MIDAS database(Highways Agency, 2007) which includes traffic information from most motorways in the United Kingdom. The real traffic data contain flow and speed measurements obtained from 6 detector stations (see Figure 15). The measurements' time interval is 60 s.

Figure 16 depicts the space-time diagrams of the real speed measurements for 3 different days: 03/06/2014, 19/06/2014 and 24/06/2014. It is observed that congestion is created upstream of the second on-ramp during the morning peak hours (between 7–8 a.m.). The created congestion spills back few kilometers upstream, without reaching the upstream end of the considered stretch. The freeway network and traffic data presented above are used to calibrate and validate the selected traffic flow models presented in Chapter 2.

4.2 Models calibration and validation

This section includes the calibration and validation results of all investigated traffic flow models. Note that the software tool CALISTO (see Section 3.2) was employed to calibrate and validate the examined models. The models were calibrated using traffic data from 03/06/2014, while the validation of the produced models was done using traffic data from 19/06/2014 and 24/06/2014. The simulation step of all examined models was set equal to $T = 5\ s$. Moreover, a single fundamental diagram was used for all motorway cells at all examined models. This implies that all motorway cells are considered to have the same characteristics, described by a common FD. Finally, it should be noted that, for each model, various calibration tests were carried out, starting the algorithm from different initial parameter vectors $\mathbf{p_0}$ (see Figure 15). The best obtained results, for each examined model, are presented in the following sections.

4.2.1 First-order model with triangular FD

A first-order model with triangular FD (CTM) was investigated first. The parameter vector under calibration consists of the free flow speed v_f, the congestion wave speed w and the critical density ρ_{cr} (see also Figure 2). Table 2 displays the optimal parameter values estimated through the calibration process, along with the minimum value of the objective function. It should be noted that during the initial calibration tests the estimated value for the parameter v_f was very low (lower than the observed free flow speed at the network). To face this fact the parameter v_f was finally considered as fixed and equal to 112 km/h. Figure 17 illustrates the space time diagram of the real speed measurements and the model's estimation of speed for the calibration day. It is observed that the reproduction of the real traffic conditions is satisfactory as the model creates the congestion at the same area and time period, as observed in the real traffic data.

Table 1 Optimal parameter values for the first-order model with triangular FD.

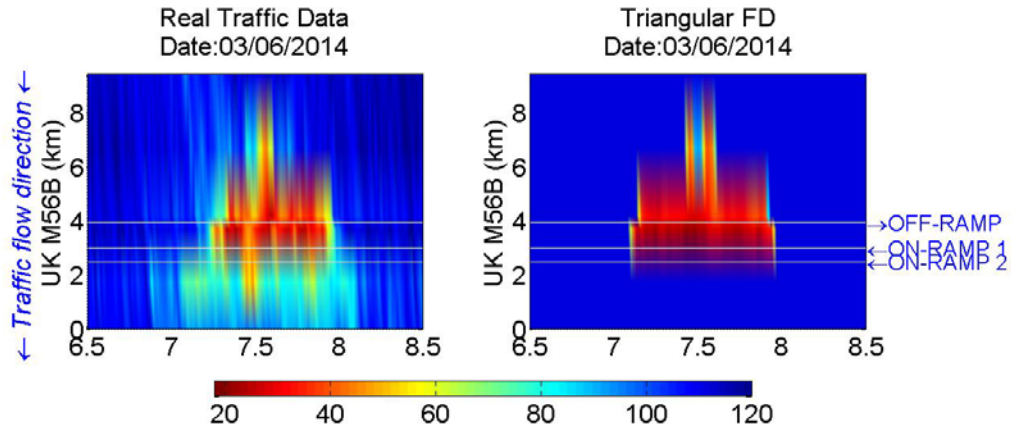| Model parameters	v_f(km/h)	w(km/h)	ρ_{cr}(veh/km/lane)
Optimal values	112	22.2	18.7
PI	18.0		

Figure 17 Space-time diagram of the real speed measurements and the first-order model with triangular FD estimation of speed for 03/06/2014.

In more detail, Figure 18 shows the time series of the real speed measurements and the corresponding model estimation of speed (for the same day) at all detector locations (see also Figure 15). It is shown here that this model estimates free flow speed at all areas outside congestion (i.e. a straight line is estimated for speed, for all periods except for congestion period). Moreover, Figure 19 presents the time series of the real flow measurements and the corresponding model estimations for all detector locations. It is observed here that the model estimations are very close to the real traffic data. However, as expected, this model is not able to reproduce the well-known capacity-drop phenomenon. See for example the model estimations at Link 6, at the time that congestion sets in.
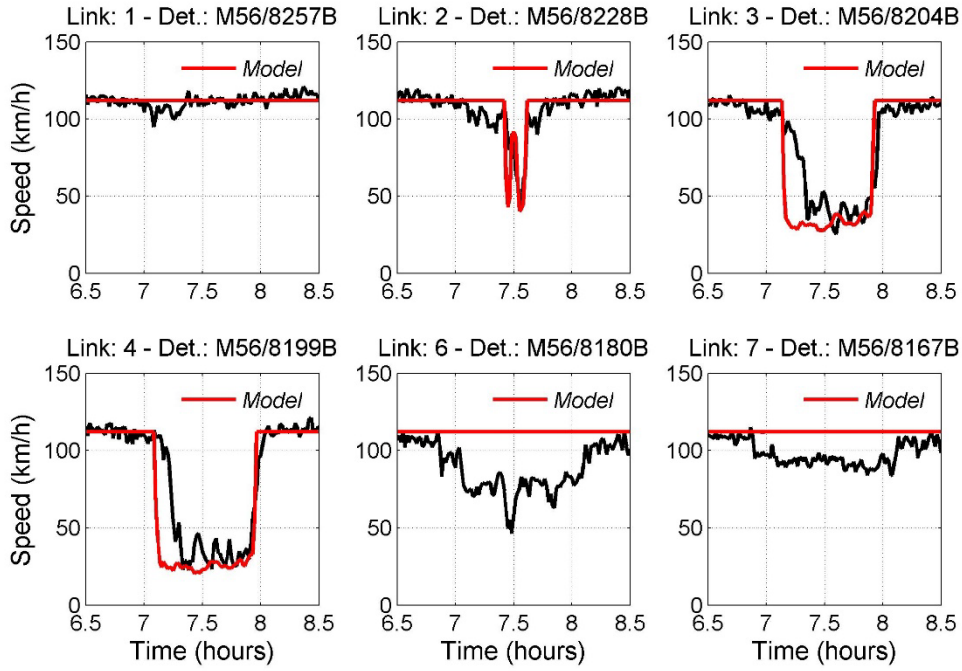
Figure 18 *Time series of the real speed measurements and the first-order model with triangular FD estimation of speed for 03/06/2014.*
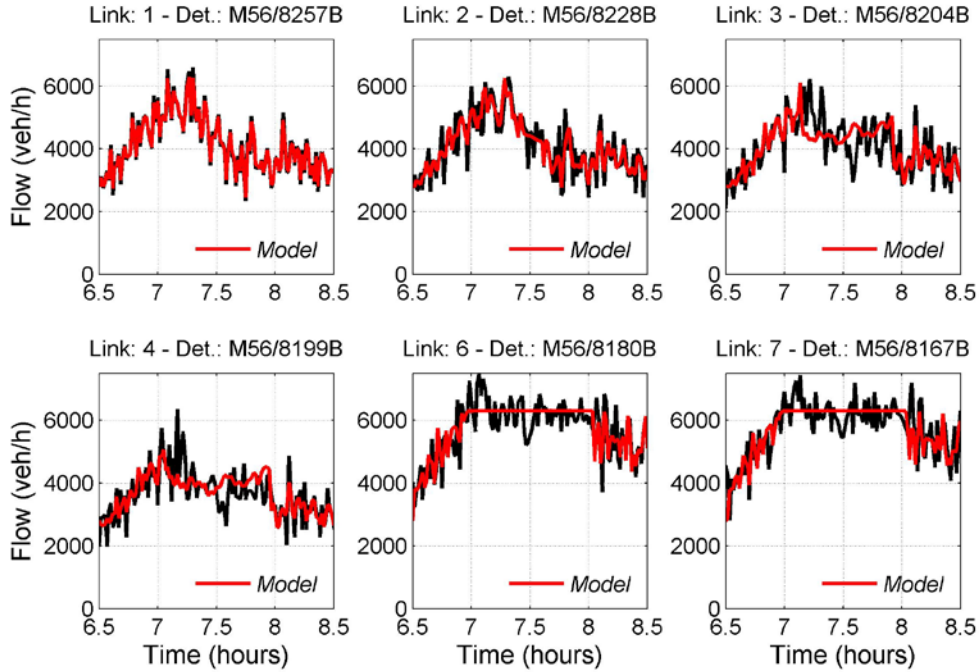

Figure 19 Time series of the real flow measurements and the first-order model with triangular FD estimation of speed for 03/06/2014.
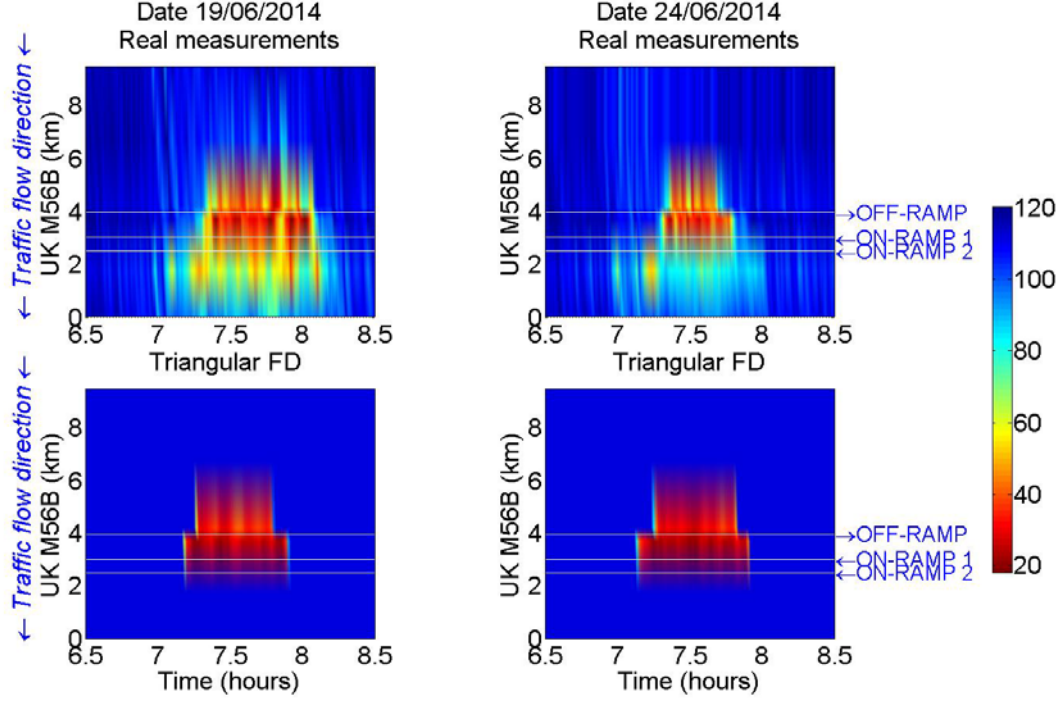
Figure 20 Space time diagram of the real speed measurements and the first-order model with triangular FD estimation of speed for 19/06/2014 and 24/06/2014.

As mentioned before, after the calibration procedure the resulted model should be validated, i.e. should be tested using different traffic data sets than the one utilized for its calibration. Figure 20 shows the space-time diagram of the real speed measurements and the model's estimation of speed for two different days, 19/06/2014 and 24/06/2014. It is observed that this model is able to reproduce the traffic conditions of this motorway stretch also for other days. In more detail, Figure 38, Figure 39, Figure 40 and Figure 41 in the Appendix, display the time series of the real speed and flow measurements and the corresponding model's estimations for these two validation dates.

4.2.2 First-order model with trapezoidal FD

The second investigated model is a first-order model with trapezoidal FD. The parameter vector under calibration consists of the free flow speed v_f, the maximum

Table 2 Optimal parameter values for first-order model with trapezoidal FD.

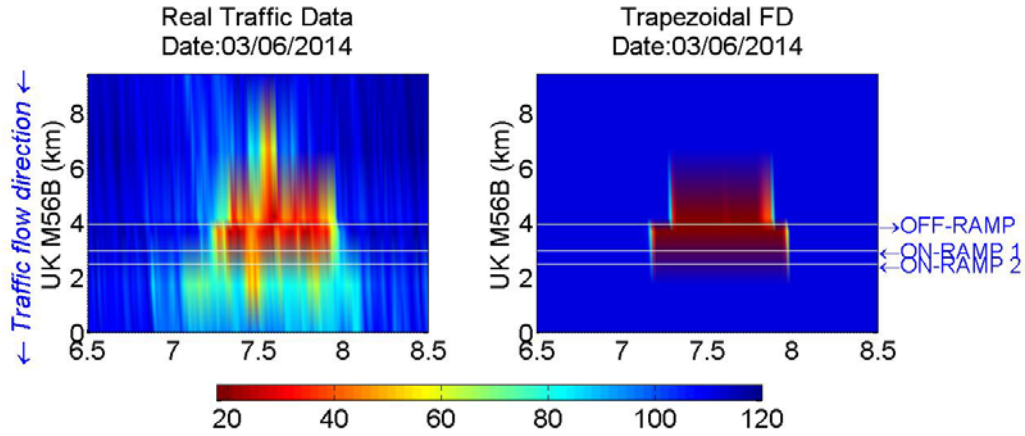| Model parameters	v_f(km/h)	ρ_{max}(veh/km/lane)	w(km/h)	Q_{cap}(veh/h)
Optimal values	112	164.5	17.4	6183
PI	18.1			

Figure 21 Space-time diagram of the real speed measurement and the first-order model with trapezoidal FD estimation of speed for 03/06/2014.

density ρ_{max}, the congestion wave speed w and the capacity flow Q_{cap} (see Figure 2).

Table 3 presents the optimal parameter values obtained through the calibration procedure. During the calibration the estimated value for the parameter v_f was very low (lower than the observed free flow speed at the network) similar to the first-order model with triangular FD. To face this fact the parameter v_f was again considered as fixed and equal to 112 km/h. Table 3 also contains the corresponding minimum value of the objective function. It is observed that the obtained PI value is very close to the PI value of the first order model with triangular FD. Figure 22 displays the space time diagram of the real speed measurements and the model's estimation of speed for the calibration day (03/06/2014). It is observed that also this model is able to reproduce the traffic conditions in this motorway stretch with sufficient accuracy creating the congestion at the right place and for the right duration.
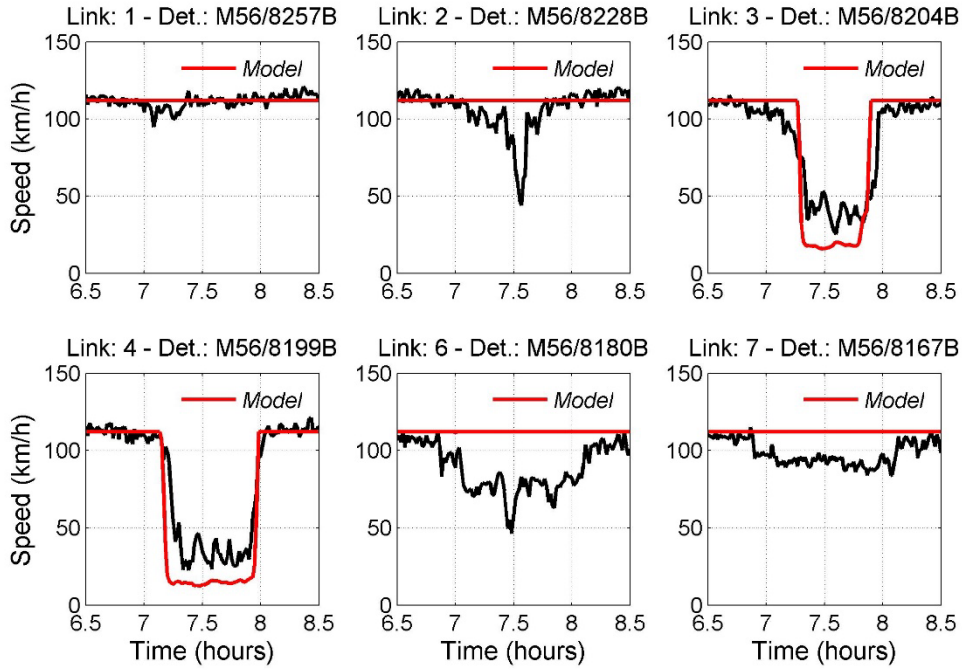
Figure 22 Time series of the real speed measurements and the first-order model with trapezoidal FD estimation of speed for 03/06/2014.
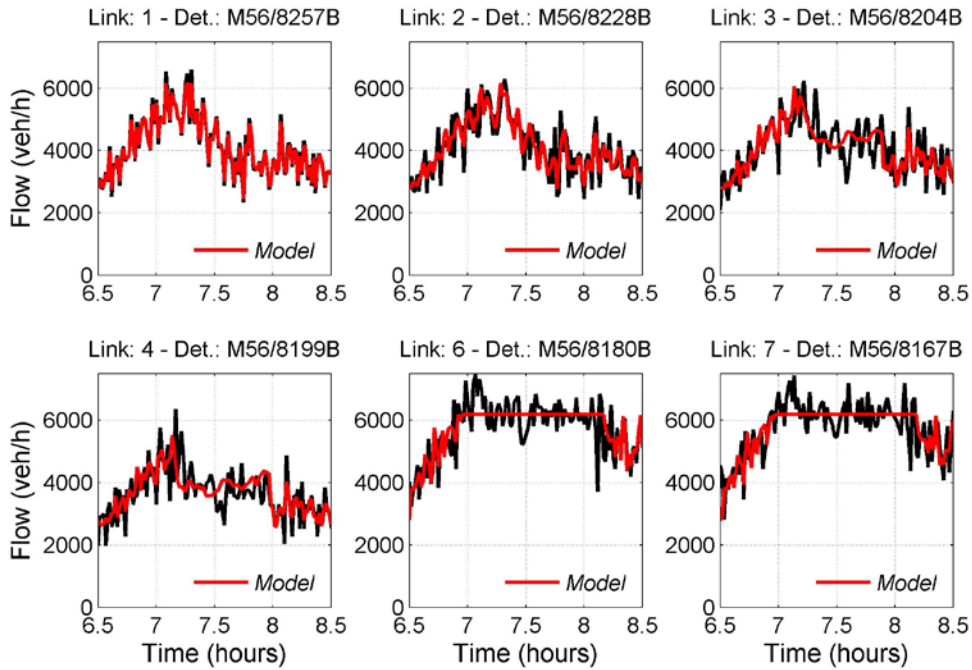

Figure 23 Time series of the real flow measurements and the first-order model with trapezoidal FD estimation of flow for 03/06/2014.
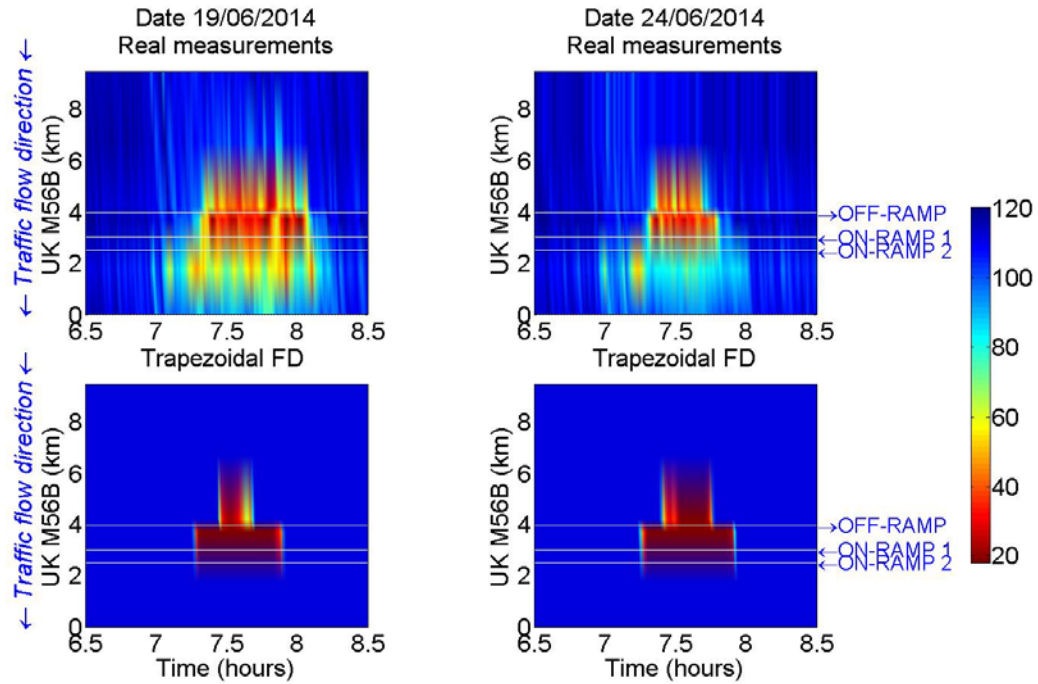
Figure 24 Space time diagram of the real speed measurements and the first-order model with trapezoidal FD estimation of speed for 19/06/2014 and 24/06/2014.

Figure 22 shows, in more detail, the time series of real speed measurements and the corresponding model estimation of speed for the same day. Similar to the previous model, this model estimates free flow speed at all areas outside congestion. Furthermore, Figure 23 depicts the time series of the real flow measurements and the corresponding model estimations for the same day. It is observed that the model estimations are very close to the real traffic data without, though, reproducing the capacity drop phenomenon.

The resulted model was validated using real data from 19/06/2014 and 24/06/2014. Figure 24 shows the space-time diagram of the real speed measurements and the model's estimation of speed for the two days. It is observed that the model is able to reproduce the traffic conditions of this motorway stretch also for other days. In more detail, Figure 42, Figure 40, Figure 42 and Figure 43, in the Appendix display the time series of the real speed and flow measurements and the corresponding model's estimations for these two validation dates.

Table 3 Optimal parameter values for the first-order model with piecewise linear FD.

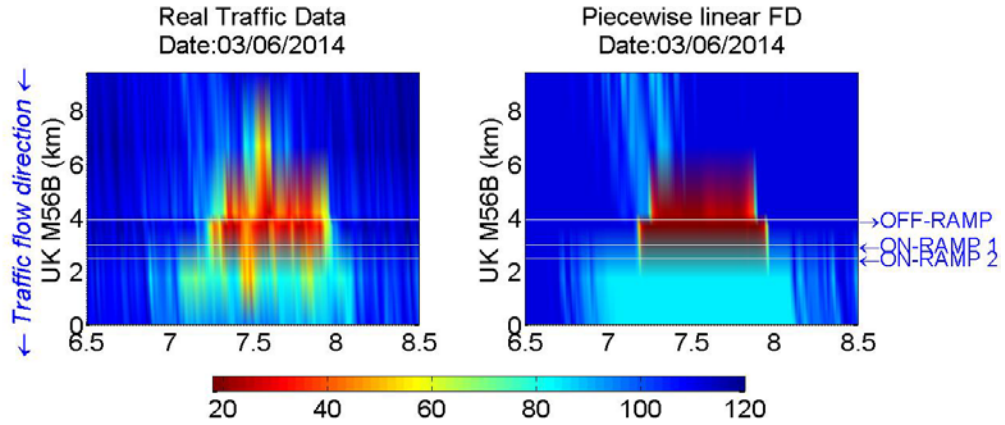| Model parameters	v_f (km/h)	ρ_{cr} (veh/km/lane)	ρ_a (veh/km/lane)	w (km/h)	Q_{cap} (veh/h)
Optimal values	111.6	24.6	14.2	14.8	6260
PI	12.6				

Figure 25 Space-time diagram of the real speed measurements and the first-order model with piecewise linear FD estimation of speed for 03/06/2014.

4.2.3 First-order model with piecewise linear FD

The third examined model is a first-order model with piecewise linear FD. The parameter vector under calibration consists of the free flow speed v_f, the congestion wave speed w ,the critical density ρ_{cr}, the capacity flow Q_{cap} and the density ρ_a (see Figure 2).

Table 4 presents the optimal parameter values obtained through the calibration procedure and the corresponding objective function value. It is observed that the obtained PI value is about 30 % lower compared to the PI of the first two models. Figure 25 displays the space time diagram of the real speed measurements and the model's estimation of speed for the calibration day. It is observed that the model's estimations are close to the real traffic data, not only during the congested period but also during the uncongested period.
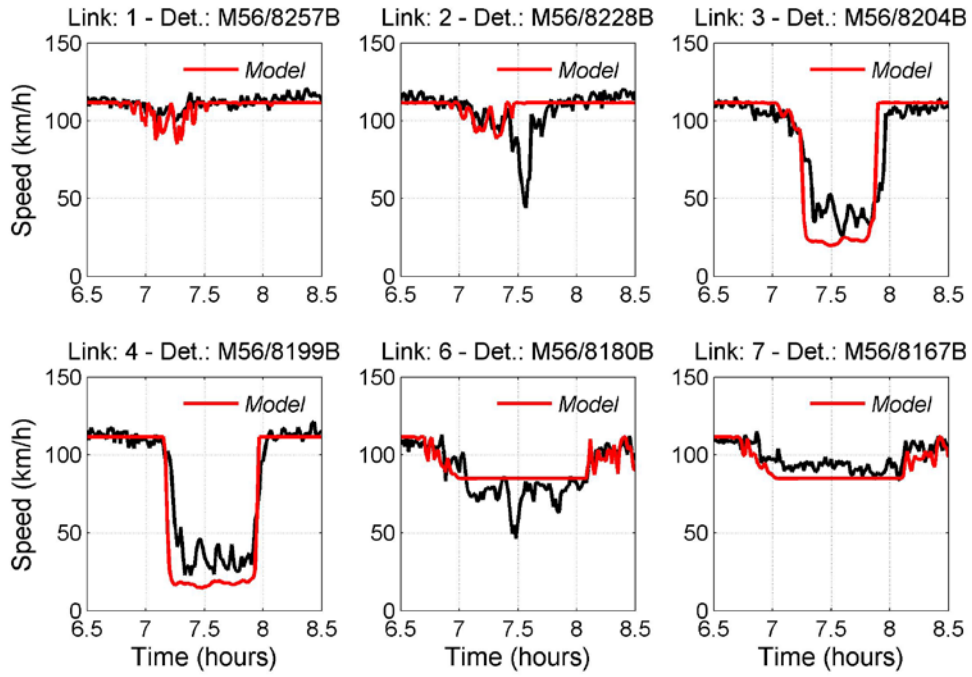
Figure 26 Time series of real speed measurement and the first-order model with piecewise linear FD estimation of speed for 03/06/2014.
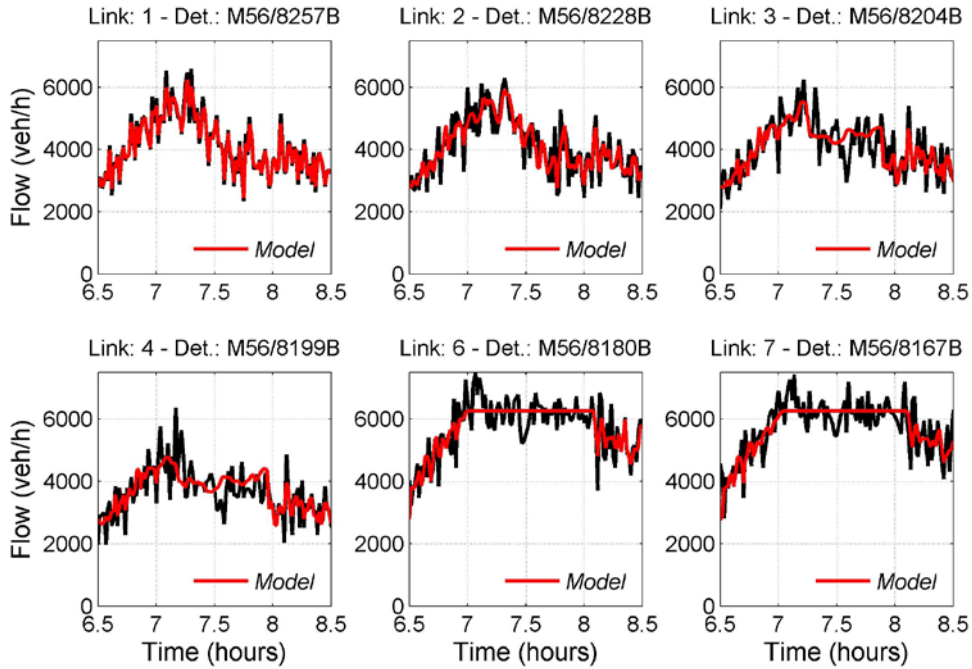

Figure 27 Time series of real flow measurement and the first-order model with piecewise linear FD estimation of flow for 03/06/2014.
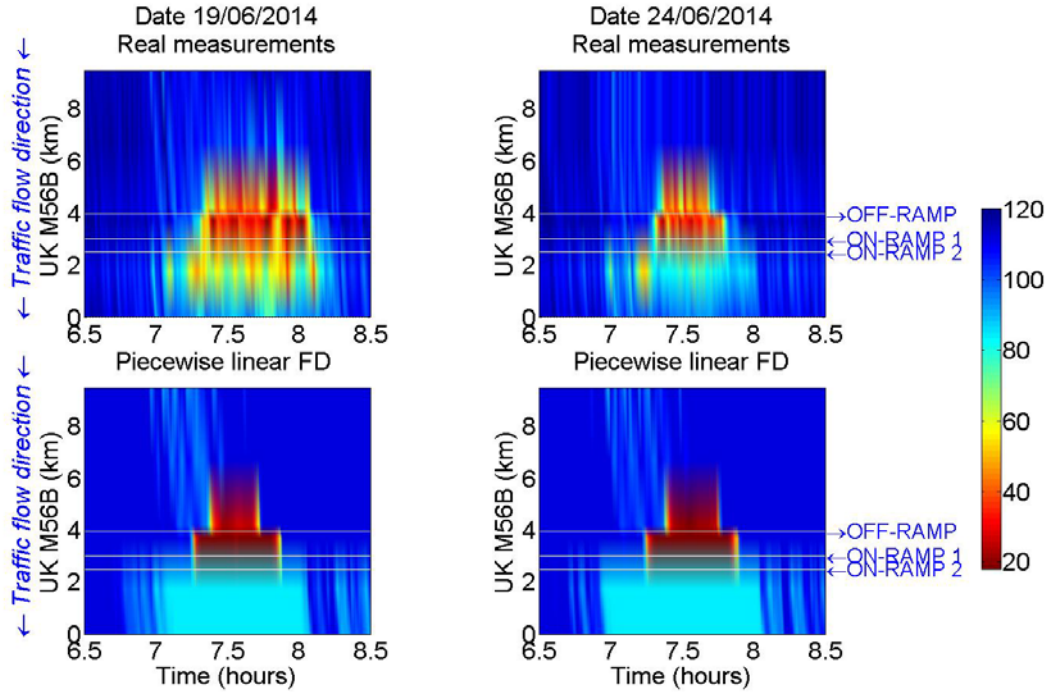
Figure 28 Space-time diagram of the real measurements of speed and the first-order model with piecewise linear FD estimation of speed for 19/06/2014 and 24/06/2014.

In more detail, Figure 26 show the time series of the real speed measurements and the corresponding model estimation of speed at different detector locations for the same day. It is shown here that, in contrast to the first two models, this model calculates lower speed than the free flow speed, downstream of the congestion creation area; see for example the speed estimations at Link 6 and 7, between 7–8 a.m. This is due to the utilized FD shape, where for densities in the range $[\rho_a, \rho_{cr}]$ the mean speed is lower than the free flow speed v_f (see also Figure 2). Moreover, Figure 27 presents the time series of the real flow measurements and the corresponding model estimations for the same day. Compared to the previous models, the model estimations are closer to the real traffic data; however, as with the other two models, it is not able to reproduce the capacity-drop phenomenon.

The obtained model was validated using real traffic data from 19/06/2014 and 24/06/2014. It is shown here that this model is able to reproduce the traffic conditions of this motorway stretch for other days, allowing for mean speed variations outside of the congestion area. In more detail, Figure 46, Figure 47, Figure

48 and Figure 49 in the Appendix, display the time series of the real speed and flow measurements and the corresponding model's estimations for the validation dates.

4.2.4 First-order model with nonlinear FD

The forth investigated model is a first-order model with nonlinear FD. The parameter vector under calibration consists of the free flow speed v_f, the congestion wave speed w ,the critical density ρ_{cr} and the capacity flow Q_{cap}. Table 5 presents the estimated optimal parameter values and the obtained PI value through the calibration procedure.

Figure 29 displays the space time diagram of the real speed measurements and the model's estimation of speed for the calibration day (03/06/2014). It is observed here that the model achieves an accurate representation of the prevailing traffic conditions and, similar to the model with piecewise linear FD, allows for mean speed variations outside of the congestion area.

Table 4 Optimal parameter values for the first-order model with nonlinear FD.

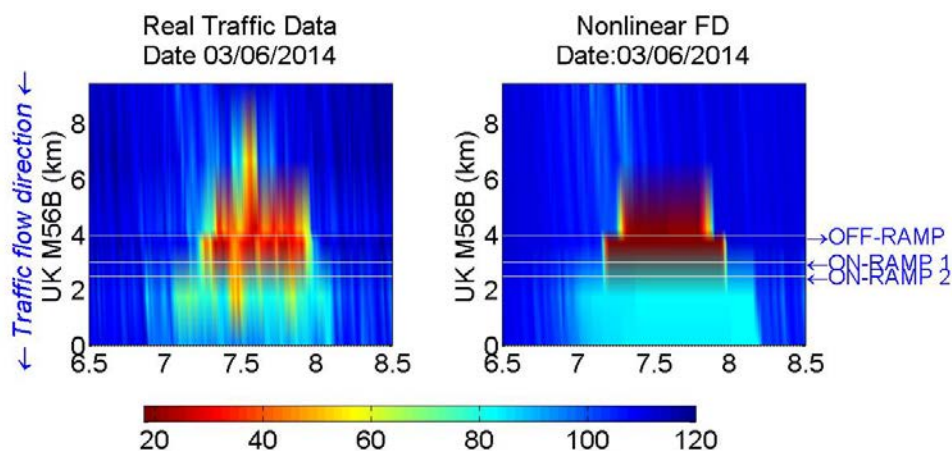| Model parameters	v_f(km/h)	ρ_{cr}(veh/km/lane)	w(km/h)	Q_{cap}(veh/h)
Optimal values	113.3	25.1	12.2	6219
PI	12.6			

Figure 29 Space-time diagram of real speed measurements and the first-order model with nonlinear FD estimation of speed.
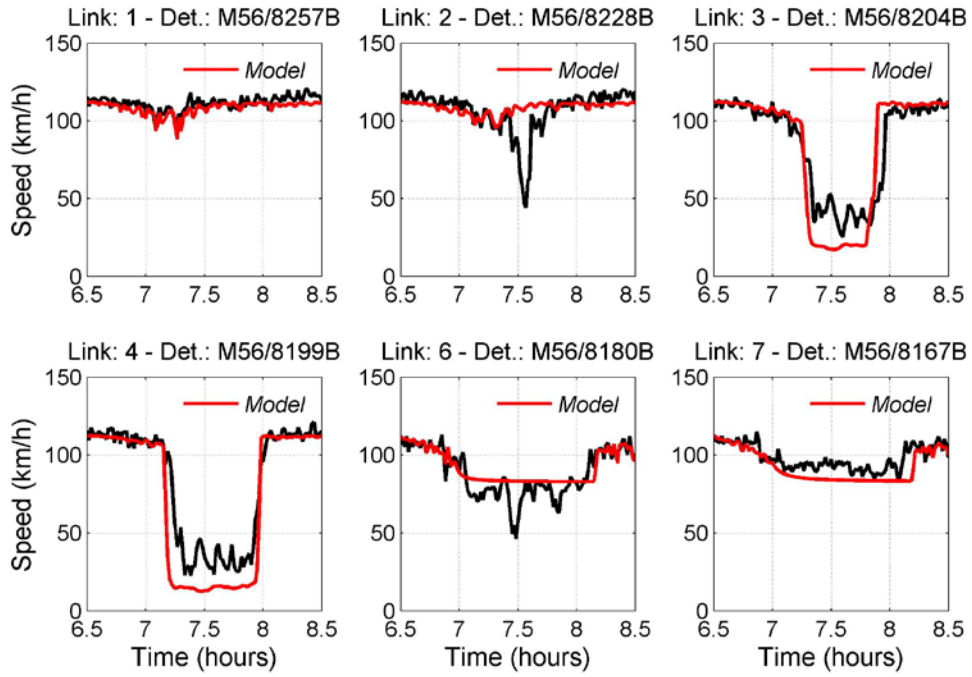
Figure 30 Time series of real speed measurement and the first-order model with nonlinear FD estimation of speed for 03/06/2014.
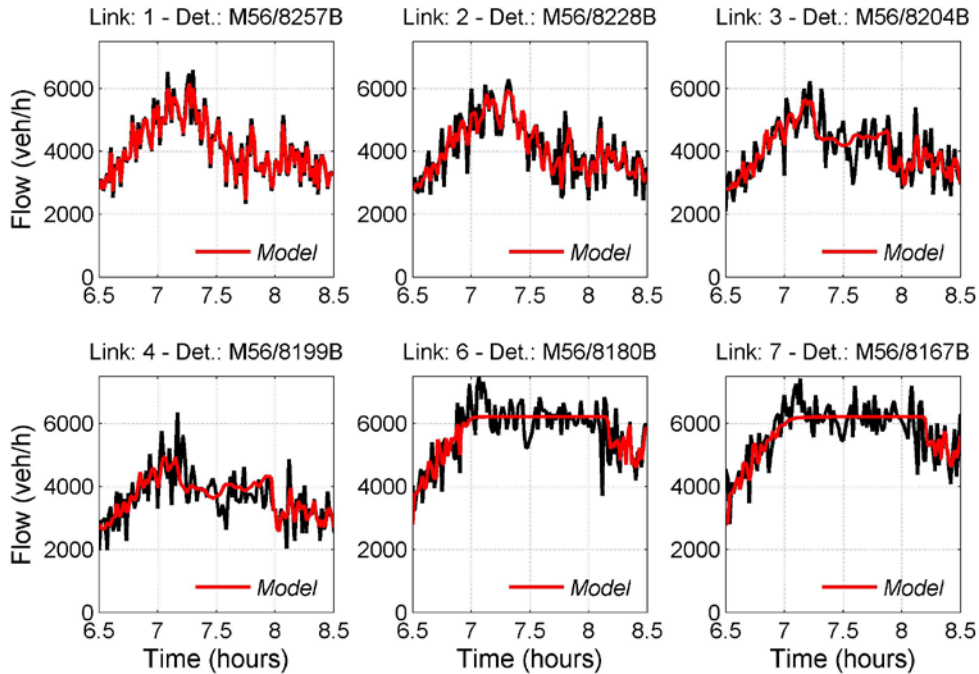

Figure 31 Time series of real flow measurement and the first-order model with nonlinear FD estimation of flow for 03/06/2014.
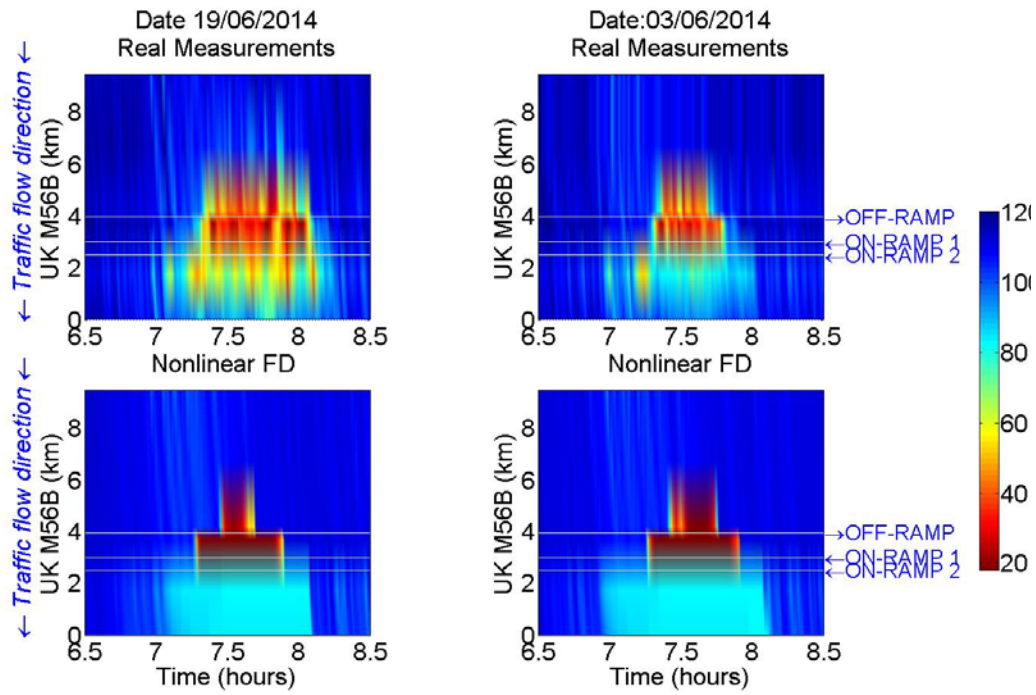
Figure 32 Space-time diagram of the real measurements of speed and the first-order model with nonlinear FD estimation of speed for 19/06/2014 and 24/06/2014.

In more detail, Figure 30 shows the time series of the real speed measurements and the corresponding model estimation of speed for the same day. Similar to the model with piecewise linear FD, this model calculates lower speed than the free flow speed, downstream of the congestion creation area; for example see the speed estimations for Link 6 and Link 7 during the congestion period. In contrast to the model with piecewise linear FD, this model calculates different speed for different undercritical densities (compare Figure 26 and Figure 30). This is a result of the utilized nonlinear FD function. Furthermore, Figure 31 shows the time series of flow measurements and the model's estimations for the calibration day. As with the previous models, the estimations are similar to the real flow measurements; however, also this model is not able to reproduce the capacity drop phenomenon.

The model was validated using real traffic data from different dates (19/06/2014 and 24/06/2014). Figure 32 shows that the model reproduces the traffic conditions of the motorway stretch for the validation days, allowing for mean speeds variations outside the congestion area, similar to the model with the piecewise linear FD. In the Appendix the time series of the real speed and flow measurements and the

46

corresponding model's estimations for the validation days are presented with detail in Figure 50, Figure 51, Figure 52 and Figure 53.

4.2.5 METANET

Finally, a second-order model is investigated for comparison purposes. The parameter vector under calibration consists of the free flow speed v_f, the critical density ρ_{cr} and the parameters α, τ, ν and δ. Table 6 displays the optimal parameter values estimated through the calibration process, along with the minimum value of the objective function. Figure 33 presents the space-time diagram of the real speed measurements and the models' estimations. It is shown that the model's estimations are very close to the real traffic conditions observed.

Table 5 Optimal parameter values for the second-order model METANET.

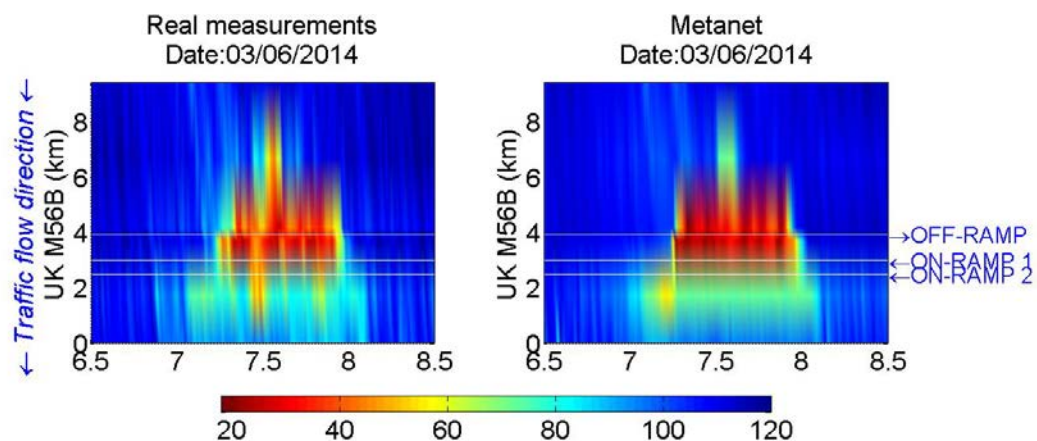| Model parameters	v_f(km/h)	ρ_{cr}(veh/km/lane)	α	τ(s)	ν(km²/h)	δ(h/km)
Optimal values	114,1	28,8	2,5	28,9	47,8	0,1
PI	7,7					

Figure 33 Space-time diagram of the real speed measurements and the second-order model METANET estimation of speed for 03/06/2014.
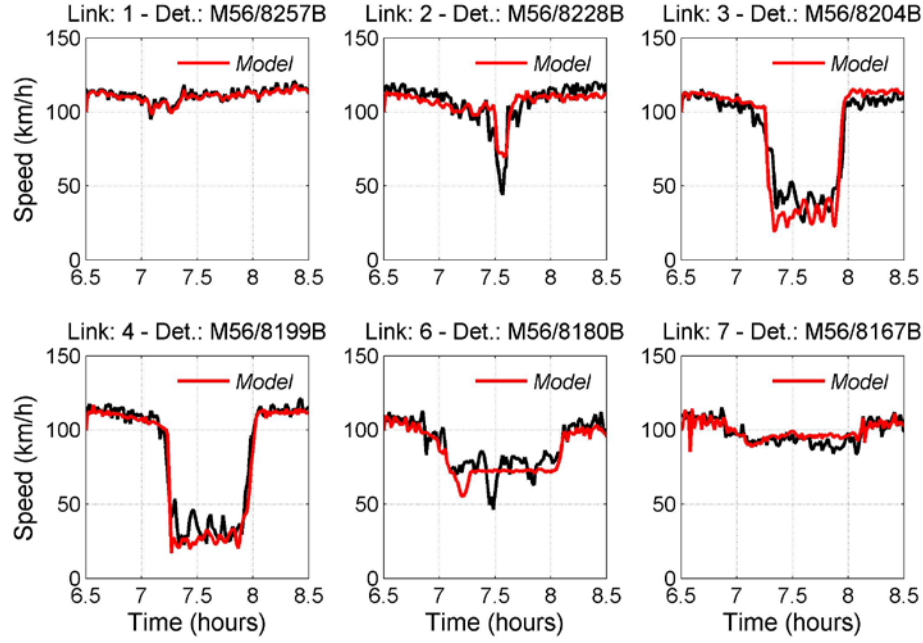
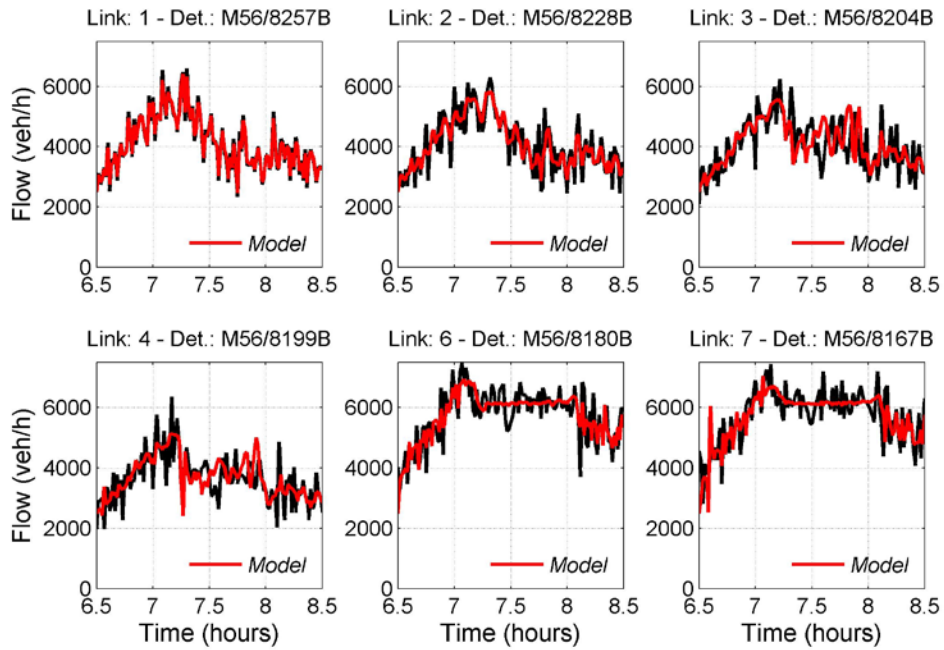*Figure 34 Time series of real speed measurements and the METANET model estimation for 03/06/2014*

Figure 35 Time series of real flow measurements and the METANET model estimation for 03/06/2014
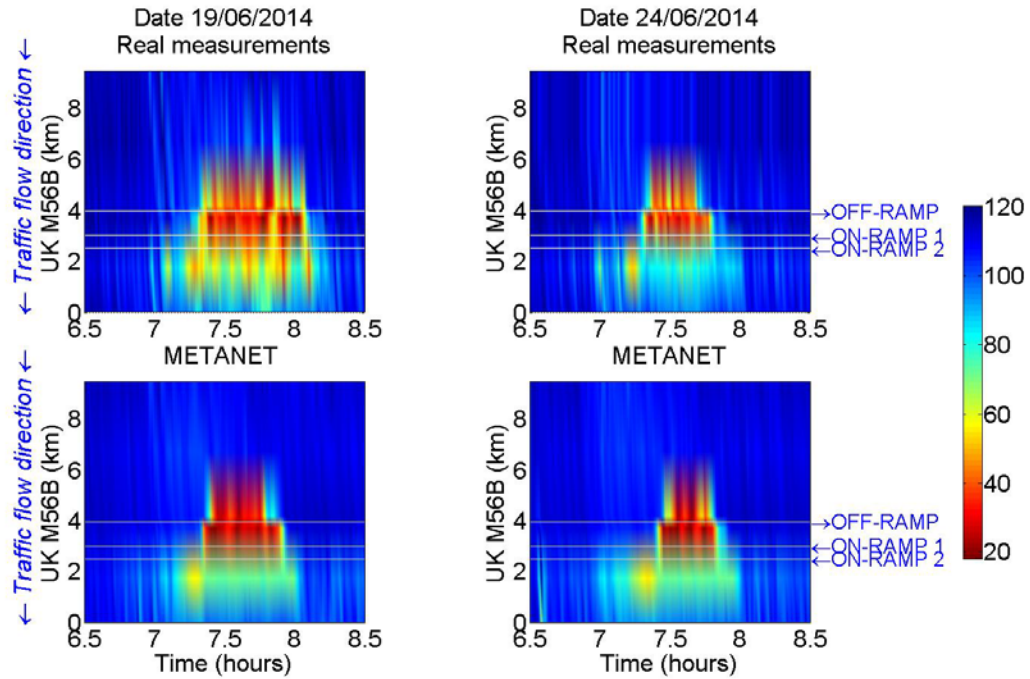
Figure 36 Space-time diagram of the real measurements of speed and the METANET model estimation of speed for 19/06/2014 and 24/06/2014.

Figure 34 shows the time series of the real speed measurements and the estimations made by the model for the calibration day. The second-order model METANET, produces a more realistic representation of the prevailing traffic conditions thanks to the fact that this model takes into account factors such as the vehicle acceleration capabilities and the drivers' reaction time. Additionally, Figure 35 presents the real flow measurements and the METANET model estimations for 03/06/2014. It is observed that unlike the first-order models, METANET model is able to reproduce the capacity drop phenomenon (see the model estimation at Link 6 when congestion sets in).

The METANET model was validated using real traffic data from 19/06/2014 and 24/06/2014. It is shown here that this model is able to reproduce the traffic conditions of this motorway stretch in a realistic way also for other days. In more detail, Figure 54, Figure 55, Figure 56 and Figure 57 in the Appendix display the time series of the real speed and flow measurements and the corresponding model's estimations for these two validation dates.
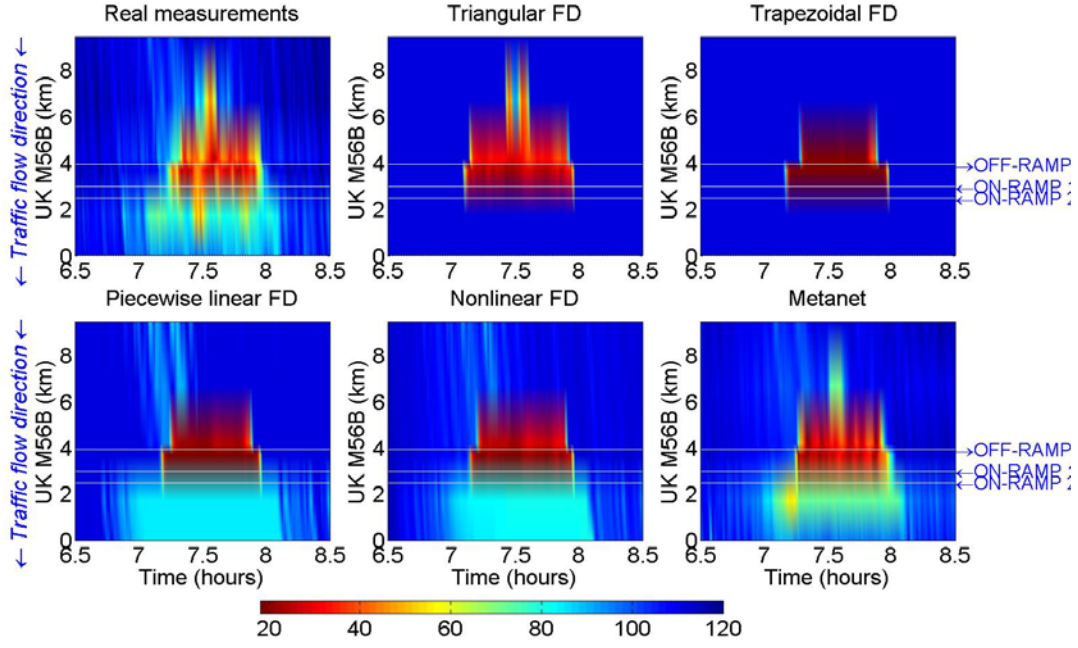
Figure 37 Space-time diagrams of the real speed measurements and the models' estimations of speed for 03/06/2014.

4.3 Models' comparison

This section summarizes and comments on the obtained results. Figure 37 presents the space time diagram of the real speed measurements and the estimations of speed for all investigated models. As described in the previous sections, the first two formulations of the LWR model (with triangular and trapezoidal FD) estimate free flow conditions outside the congestion area. The next two formulations (with piecewise linear and nonlinear FD) allow for mean speed variations, outside the congestion area, i.e. for undercritical densities, and as a result they achieve higher accuracy compared to the first two formulations. Finally, the second-order model METANET reproduces the traffic conditions with higher accuracy compared to all first-order model formulations as this model takes into account the vehicles' acceleration capabilities and the drivers' reaction time by including an extra equation to describe the speed dynamics.

Table 7 contains the estimated models' parameter values and the corresponding performance indices for the calibration and the validation days. It is observed that the four formulations of the LWR model calculated similar value for the capacity parameter (Q_{cap}). Moreover, the formulation with the triangular FD estimated the

Table 6 Calibration and validation results for all investigated models.

Model	v_f (km/h)	ρ_{cr} (veh/km /lane)	w (km/h)	Q_{cap} (veh/h)	ρ_{max} (veh/km /lane)	ρ_a (veh/km /lane)	PI 3/6	PI 19/6	PI 24/6
Trian. FD	112	18.7	22.2	6283	113.0	-	18.0	23.9	18.6
Trap. FD	112	-	17.4	6183	164.5	-	18.1	24.3	16.9
PWL FD	111.6	24.6	14.8	6260	165.4	14.2	12.6	19.2	13.0
NL FD	113.3	25.1	12.3	6219	195.4	-	12.6	19.1	13.3
METANET	114,1	28,8	-	6608	-	-	7.7	15.0	12.1

lowest value for the critical density parameter (ρ_{cr}), as it was expected. Regarding the performance indices the formulations with piecewise linear and nonlinear FD achieve higher accuracy compared to the triangular and trapezoidal in both the calibration and validation dates. Finally the second order model METANET achieves the lowest PI value compared to all first order formulations. Note that only some of the METANET parameters are displayed in Table 7, while the rest parameter values are included in Table 6.

5 Conclusions and future work

Within this thesis four first-order macroscopic traffic flow models and one second-order model were employed and examined. In particular, four different formulations of the LWR model (using different shapes for the FD) and the METANET model were calibrated and validated using real traffic data from a motorway in the UK. The models were compared regarding their ability to reproduce the prevailing traffic conditions on the motorway. The calibration and validation results showed that all investigated models were able to reproduce the real traffic data with sufficient accuracy. As it was expected, the second-order model METANET was the most accurate compared to all first-order models. Comparing the first-order model formulations, it was observed that the models using a piecewise linear or nonlinear FD were more accurate than the models using a triangular or trapezoidal FD, especially during the uncongested period. It should also be noted that none of the four first-order formulations were able to reproduce the capacity drop phenomenon, while the second-order model was able to reproduce it.

The innovative software tool CALISTO was utilized for the calibration and validation procedure. CALISTO has been recently developed and makes the calibration and validation procedure an easy task. In the utilized version of the software the examined models were programmed and introduced. Moreover, the software includes three optimization algorithms that can be used for the calibration procedure, the Nelder-Mead algorithm, a genetic algorithm and the cross-entropy method. The first optimization method was employed in the presented investigations.

Future work should aim at the improvement of the examined first-order model formulations. For example, focus on the reproduction of the capacity drop phenomenon. Moreover, the software tool CALISTO, could further be extended, by including more macroscopic traffic models, already existing or recently proposed, and also by including a bigger selection of optimization algorithms.

6 References

Daganzo, C.F., 1995. The cell transmission model, part II: Network traffic. Transp. Res. Part B Methodol. 29B, 79–93. doi:10.1016/0191-2615(94)00022-R

Daganzo, C.F., 1994. The Cell Transmission Model. Part I: A Simple Dynamic Representation of Highway Traffic. Transp. Res. Part B Methodol. 28, 269–287.

Highways Agency, 2007. Motorway Incident Detection and Automatic Signalling (MIDAS) Design Standard., 1st editio. ed. Bristol,UK.

Hoogendoorn, S.P., Bovy, P.., 2001. State-of-the-art of Vehicular Traffic Flow Modelling, Part I. J. Syst. Control Eng. 215, 283–303.

Lagarias, J.C., Reeds, J. a., Wright, M.H., Wright, P.E., 1998. Convergence Properties of the Nelder--Mead Simplex Method in Low Dimensions. SIAM J. Optim. 9, 112–147. doi:10.1137/S1052623496303470

Lighthill, M.J., Whitham, G.B., 1955. On Kinematic Waves. II. A Theory of Traffic Flow on Long Crowded Roads. Proc. R. Soc. A Math. Phys. Eng. Sci. 229, 317–345. doi:10.1098/rspa.1955.0089

Papageorgiou, M., Blosseville, J.-M., Haj-Salem, H., 1990. Modelling and real-time control of traffic flow on the southern part of Boulevard Peripherique in Paris: Part II: Coordinated on-ramp metering. Transp. Res. Part A Gen. 24, 361–370. doi:10.1016/0191-2607(90)90048-B

Papageorgiou, M., Messmer, A., 1990. METANET: a macroscopic simulation program for motorway networks. Traffic Eng. Control 31, 466–470.

Payne, H.J., 1971. Models of freeway traffic and control, in: Proc. Mathem. of Publ. Syst. Simul. Council. pp. 51–61.

Richards, P.I., 1956. Shock waves on the highway. Oper. Res. 4, 42–51.

Spiliopoulou, A., Papamichail, I., Papageorgiou, M., Chrysoulakis, J., 2014. A Calibration tool for macroscopic traffic flow models, in: Proc. of the 3rd International Symposium & 25th National Conference on Operational Research, Volos, Greece, June 26–28. pp. 215–225.

Appendix

In this Appendix the time series of the real flow and speed measurements and the corresponding models' estimations are presented for the two validation days.
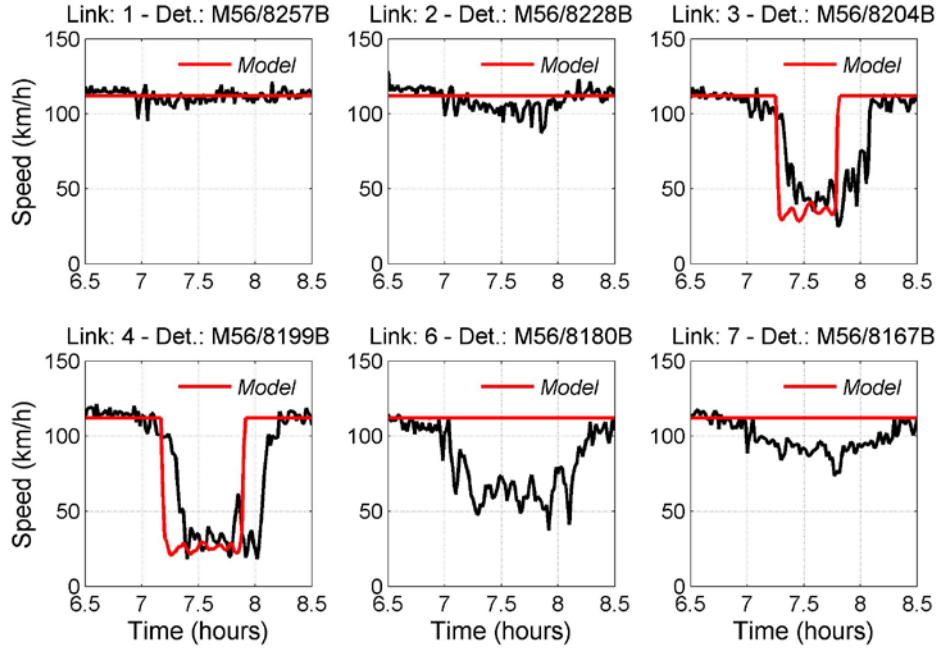

Figure 38 Time series of the real flow measurements and the first-order model with triangular FD estimation of speed for 19/06/2014.
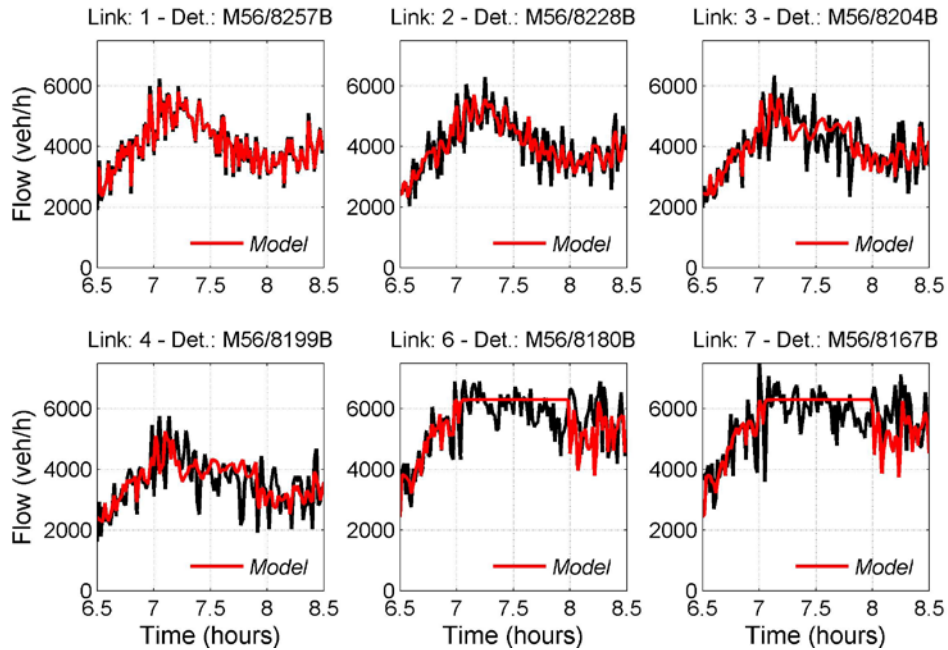

Figure 39 Time series of the real flow measurements and the first-order model with triangular FD estimation of flow for 19/06/2014.
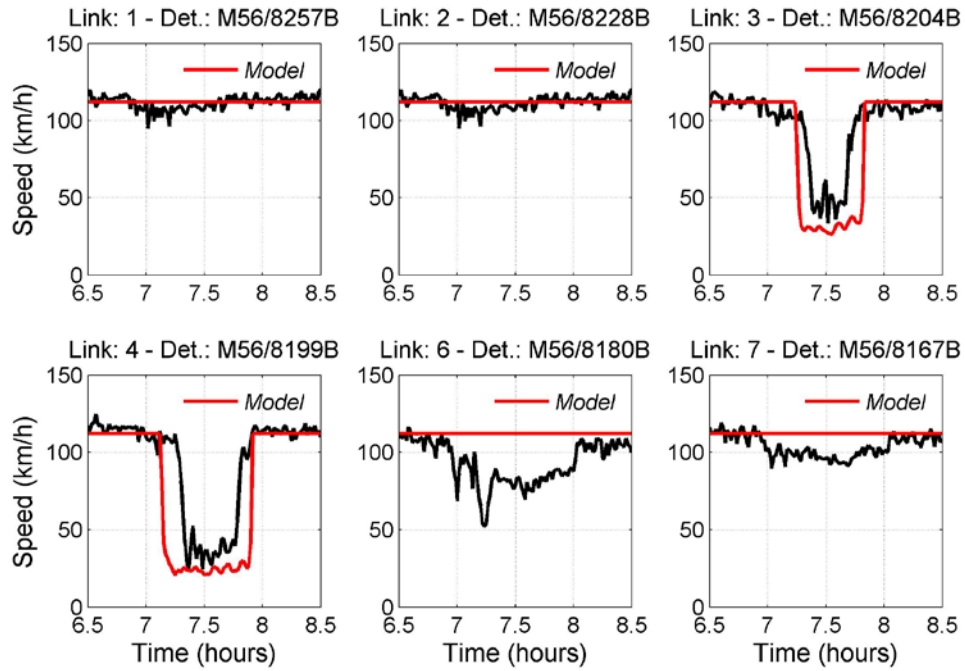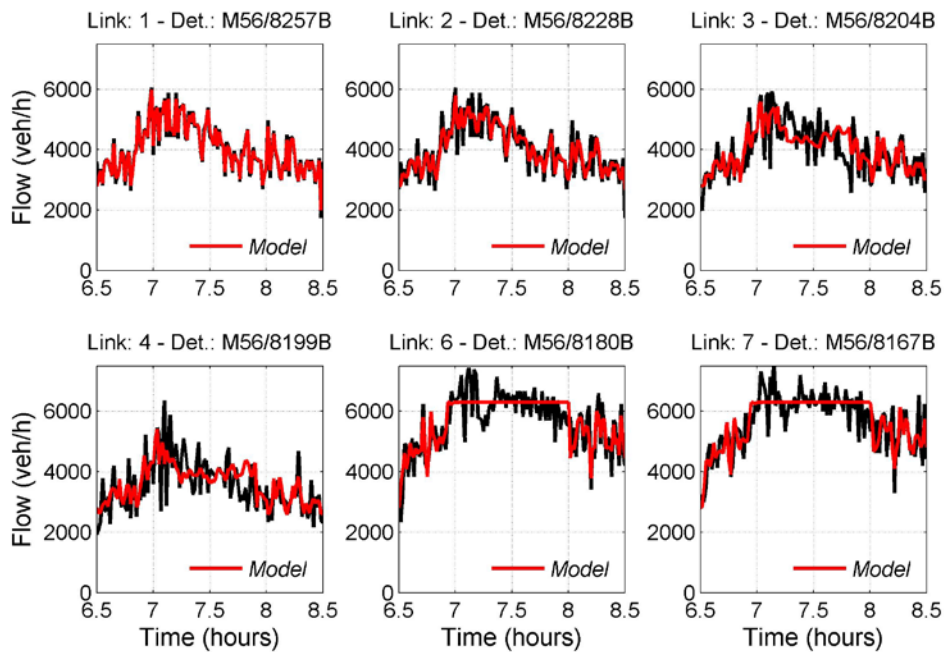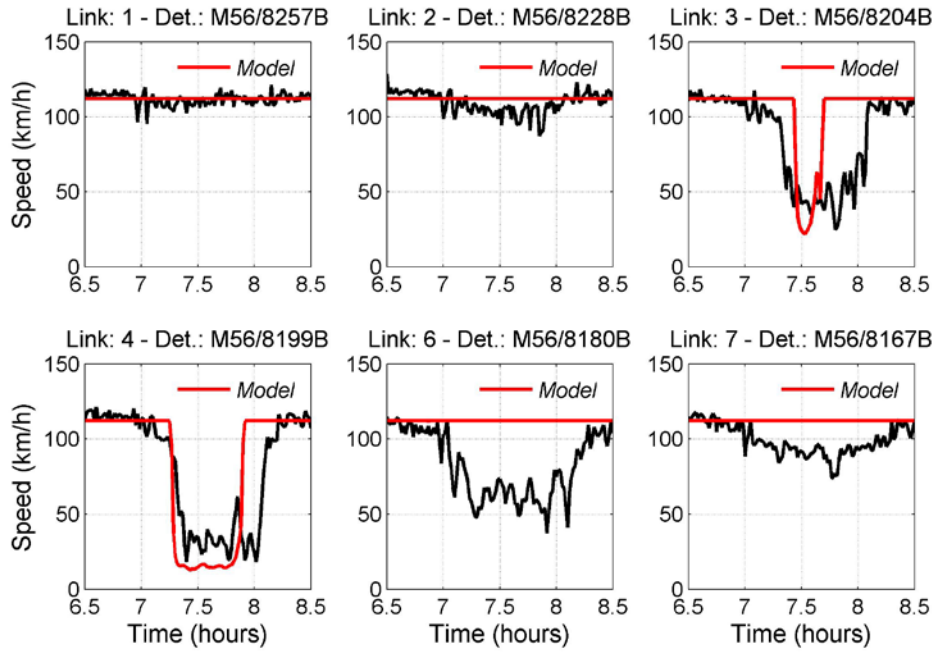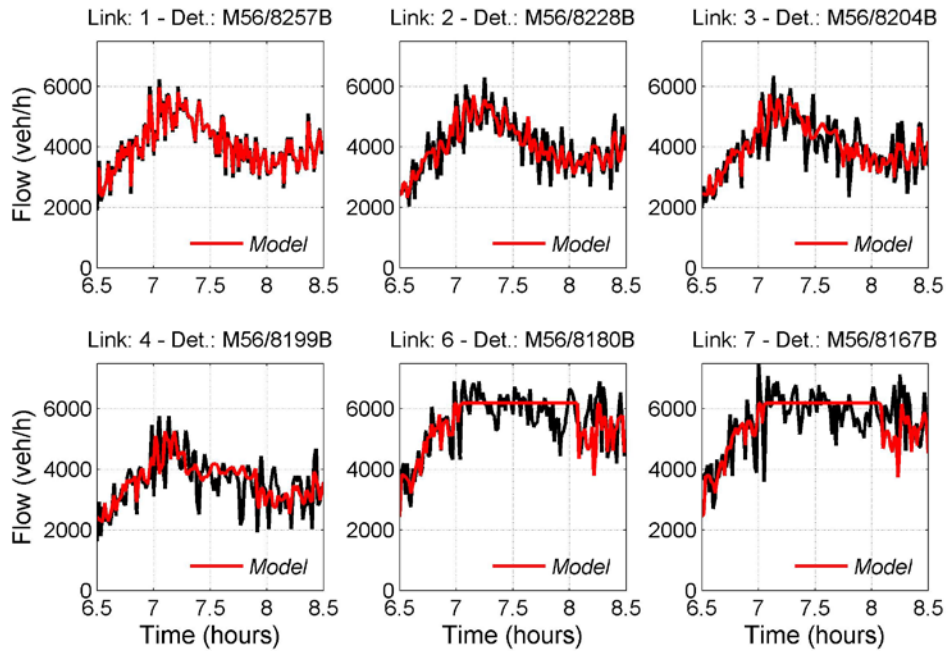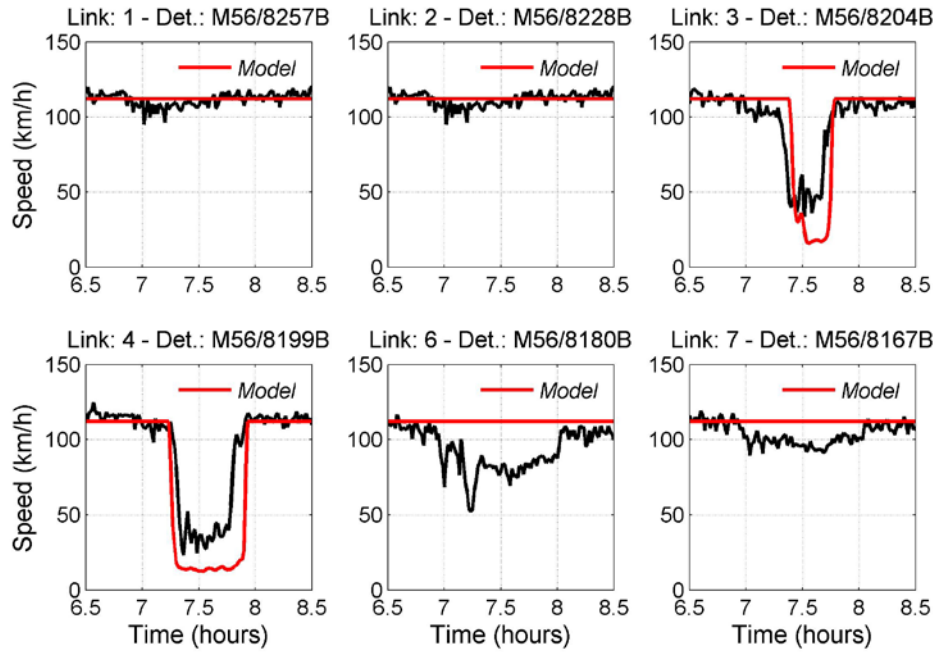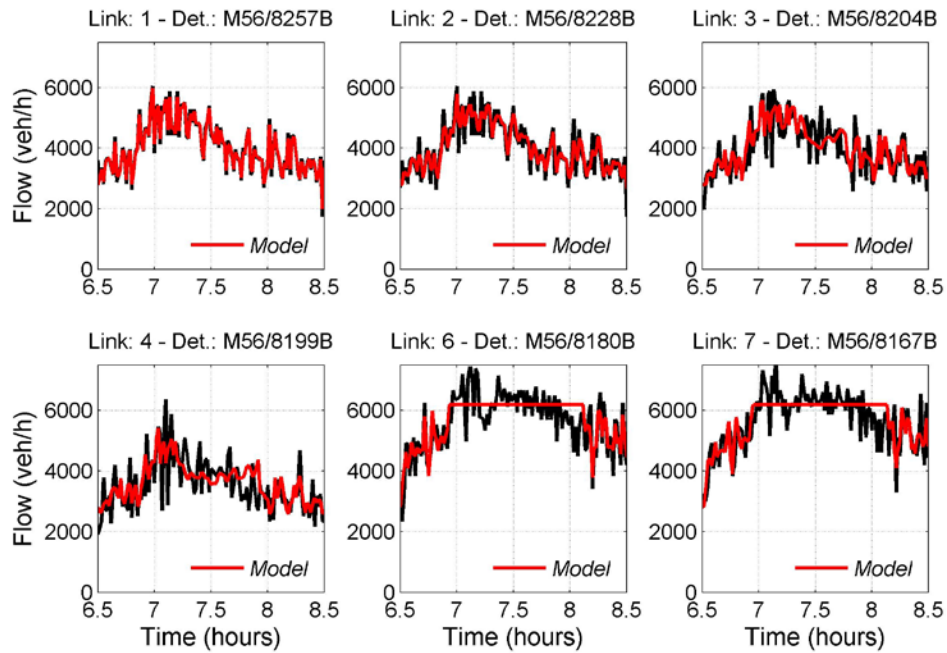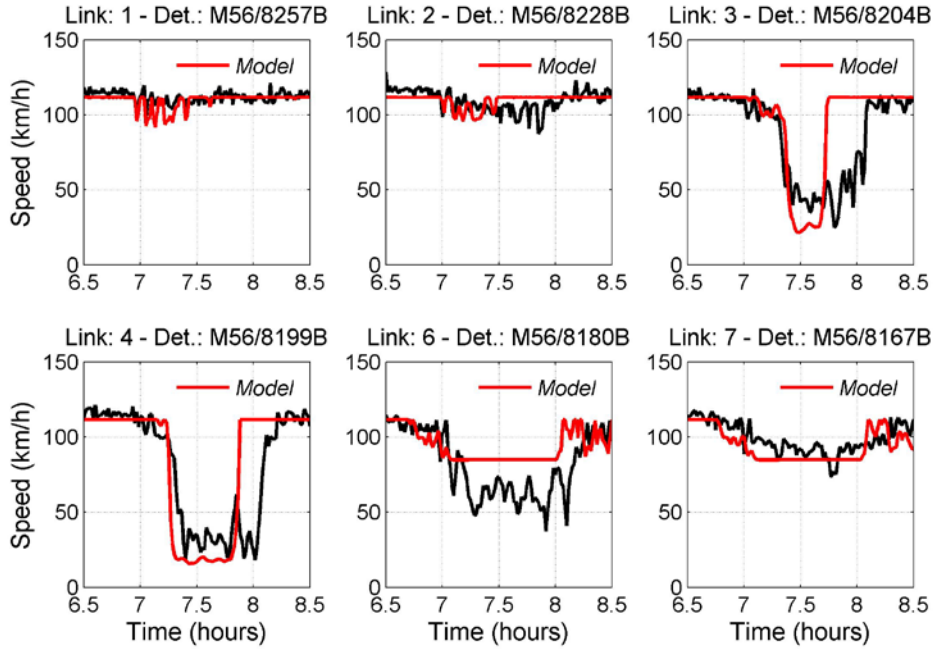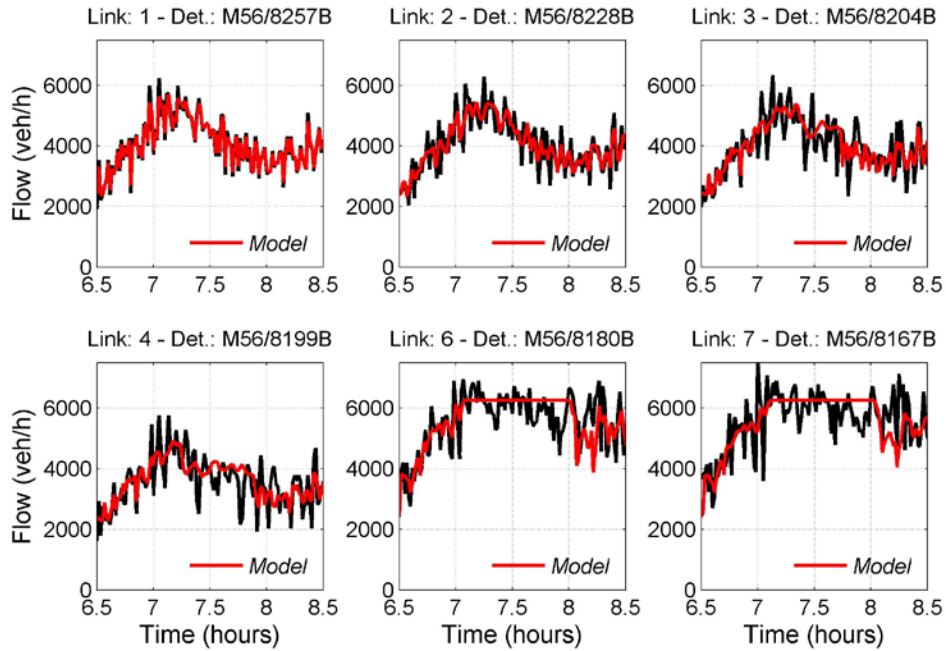
Figure 40 Time series of the real speed measurements and the first-order model with triangular FD estimation of speed for 24/06/2014.

Figure 41 Time series of the real flow measurements and the first-order model with triangular FD estimation of flow for 24/06/2014.
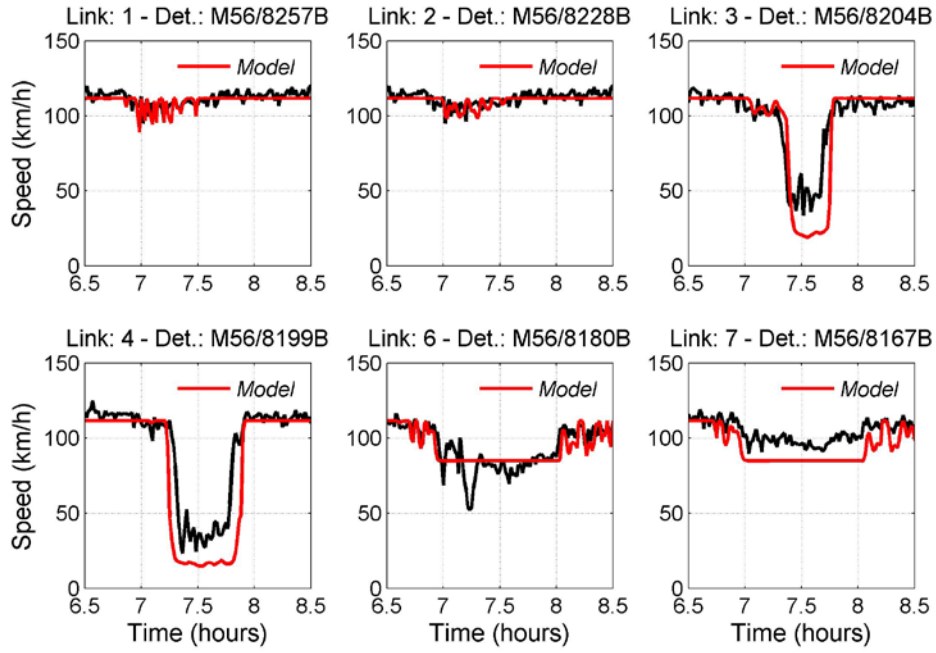
56

Figure 42 Time series of the real speed measurements and the first-order model with trapezoidal FD estimation of speed for 19/06/2014.

Figure 43 Time series of the real flow measurements and the first-order model with trapezoidal FD estimation of flow for 19/06/2014.

Figure 44 Time series of the real speed measurements and the first-order model with trapezoidal FD estimation of speed for 24/06/2014.
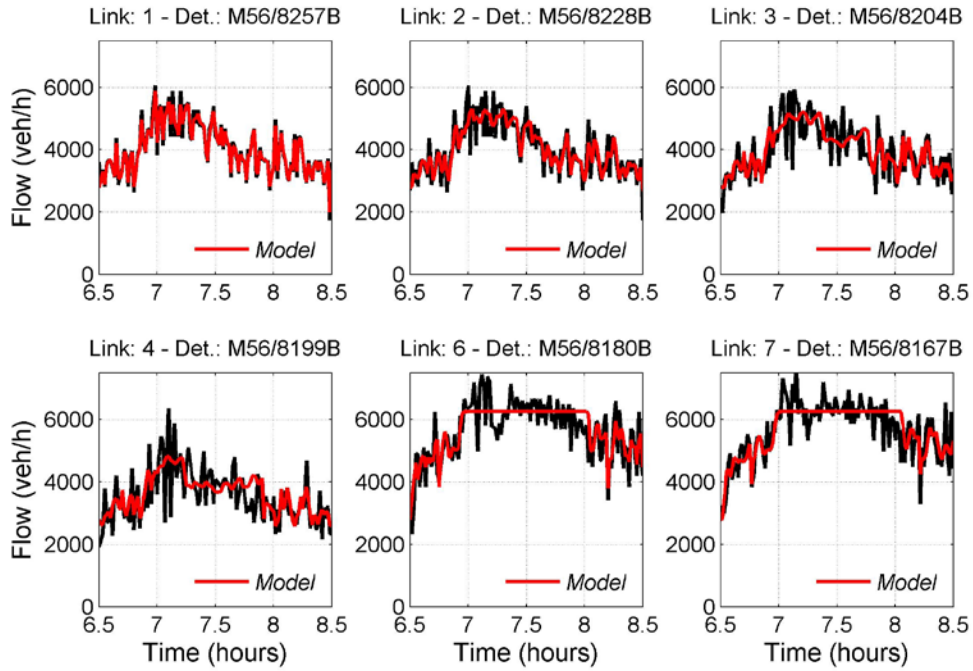

Figure 45 Time series of the real flow measurements and the first-order model with trapezoidal FD estimation of flow for 24/06/2014.

58

Figure 46 Time series of the real speed measurements and the first-order model with piecewise linear FD estimation of speed for 19/06/2014.

Figure 47 Time series of the real flow measurements and the first-order model with piecewise linear FD estimation of flow for 19/06/2014.
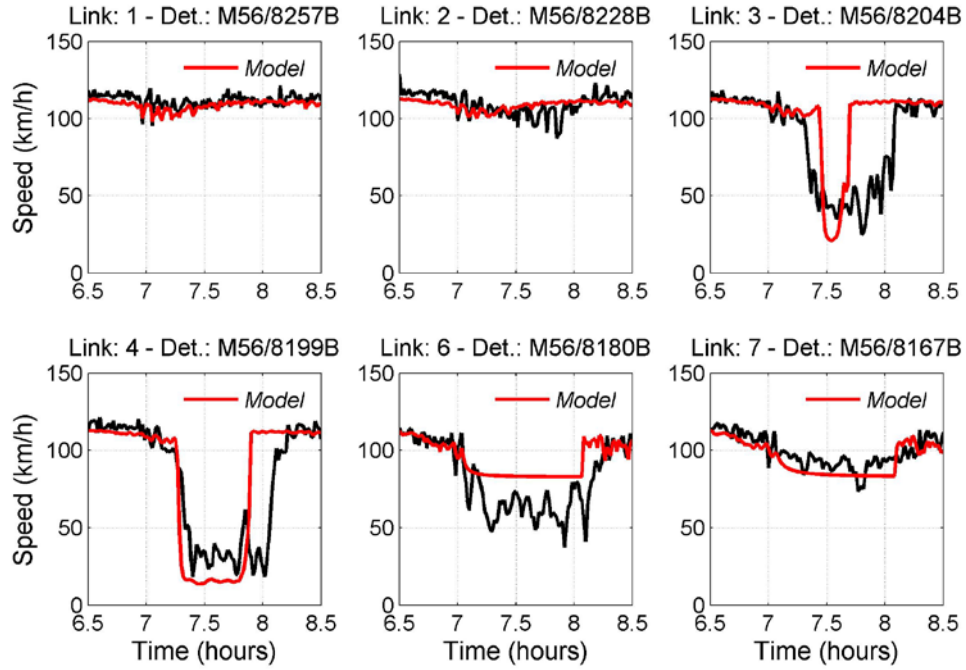
Figure 48 Time series of the real speed measurements and the first-order model with piecewise linear FD estimation of speed for 24/06/2014.

Figure 49 Time series of the real flow measurements and the first-order model with piecewise linear FD estimation of flow for 24/06/2014.

Figure 50 Time series of the real speed measurements and the first-order model with nonlinear FD estimation of speed for 19/06/2014.
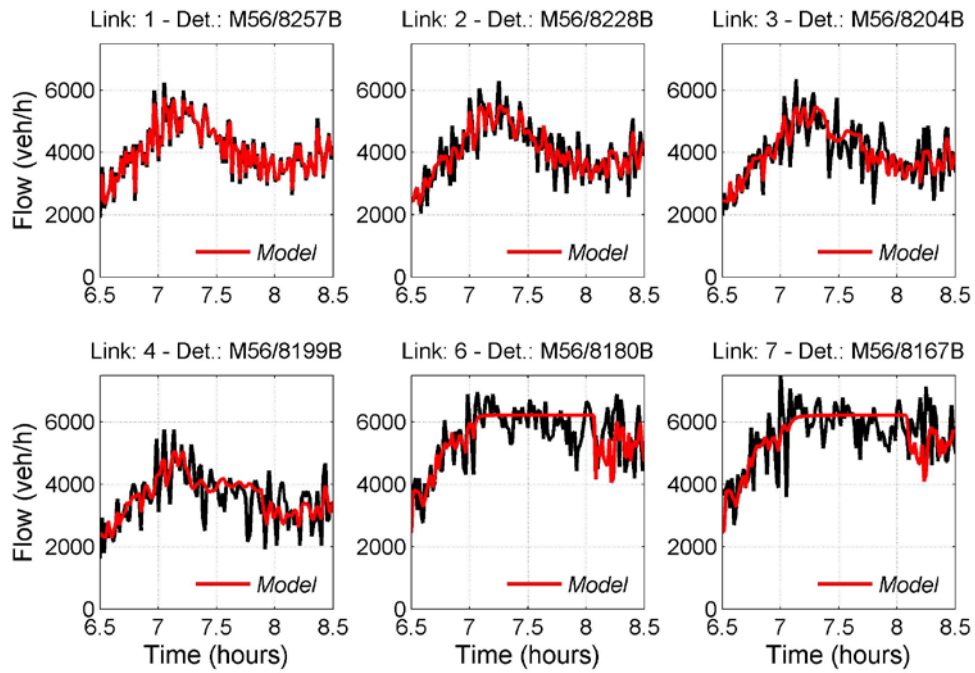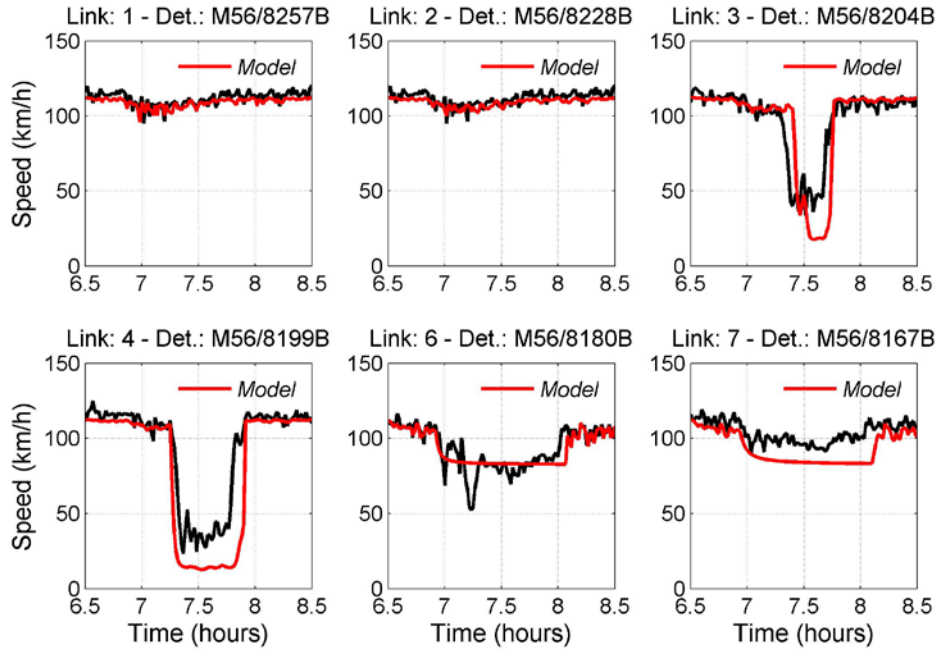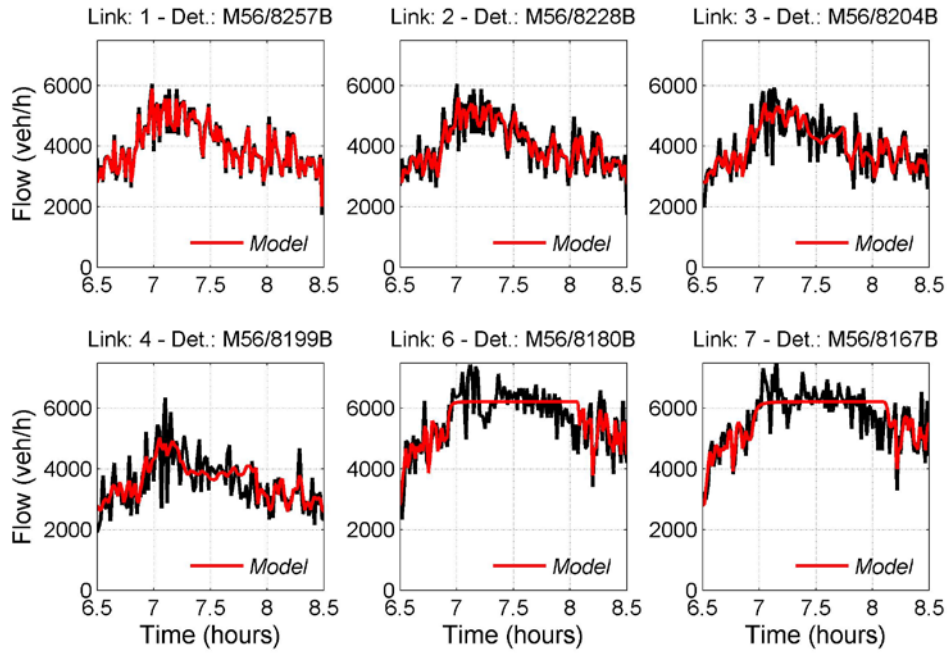

Figure 51 Time series of the real flow measurements and the first-order model with nonlinear FD estimation of flow for 19/06/2014.

Figure 52 Time series of the real speed measurements and the first-order model with nonlinear FD estimation of speed for 24/06/2014.

Figure 53 Time series of the real flow measurements and the first-order model with nonlinear FD estimation of flow for 24/06/2014.
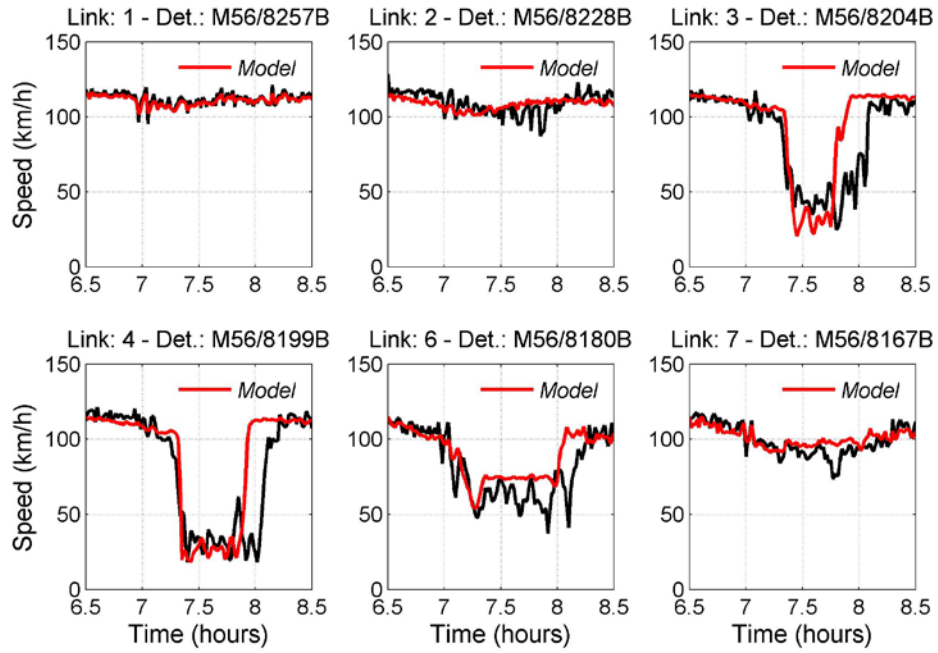
Figure 54 Time series of the real speed measurements and the second-order model METANET estimation of speed for 19/06/2014.
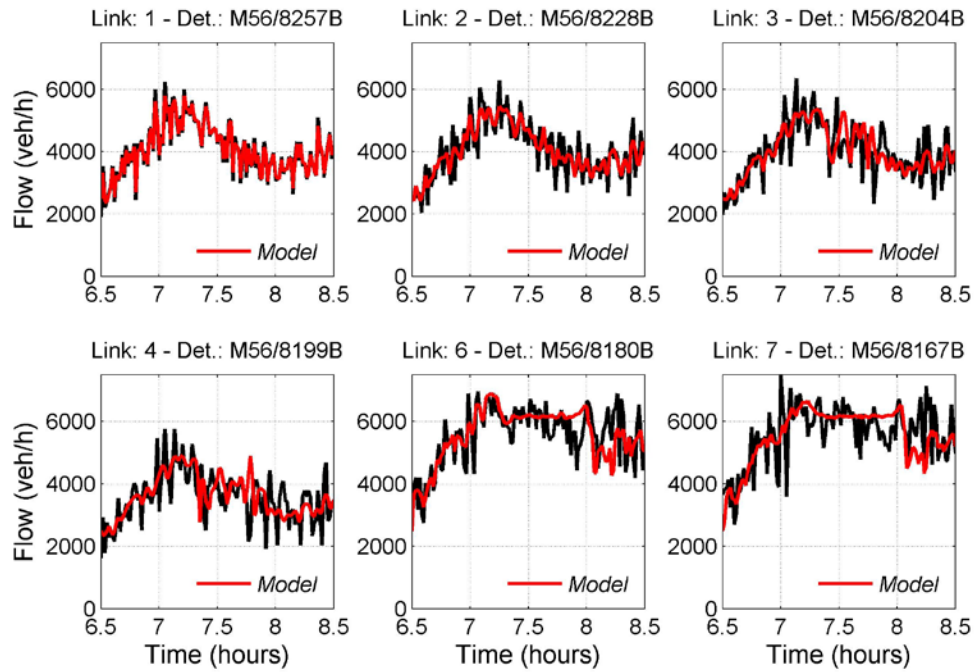

Figure 55 Time series of the real flow measurements and the second-order model METANET estimation of flow for 19/06/2014.
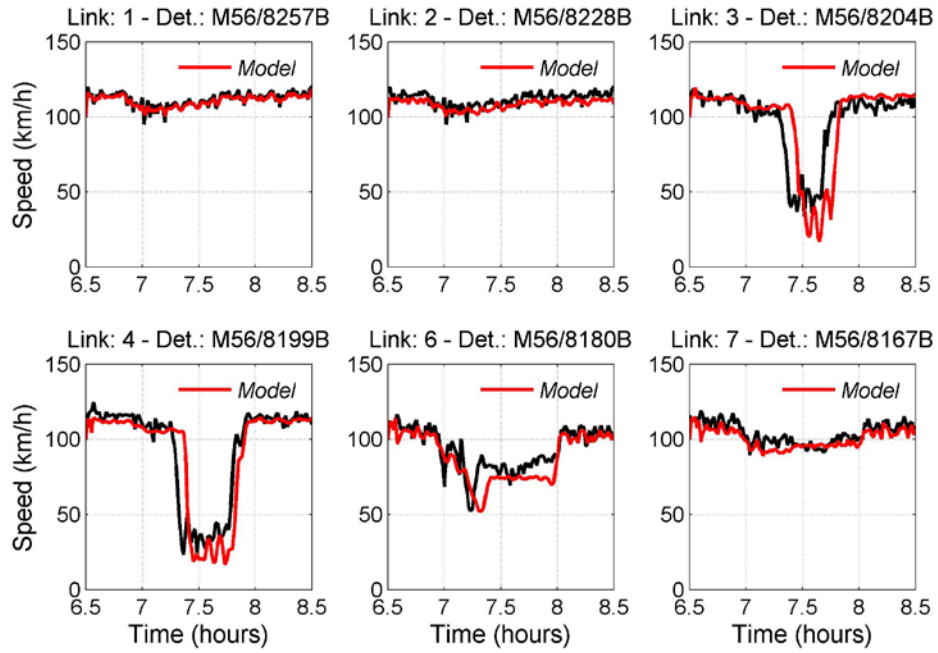
Figure 56 Time series of the real speed measurements and the second-order model METANET estimation of speed for 24/06/2014.
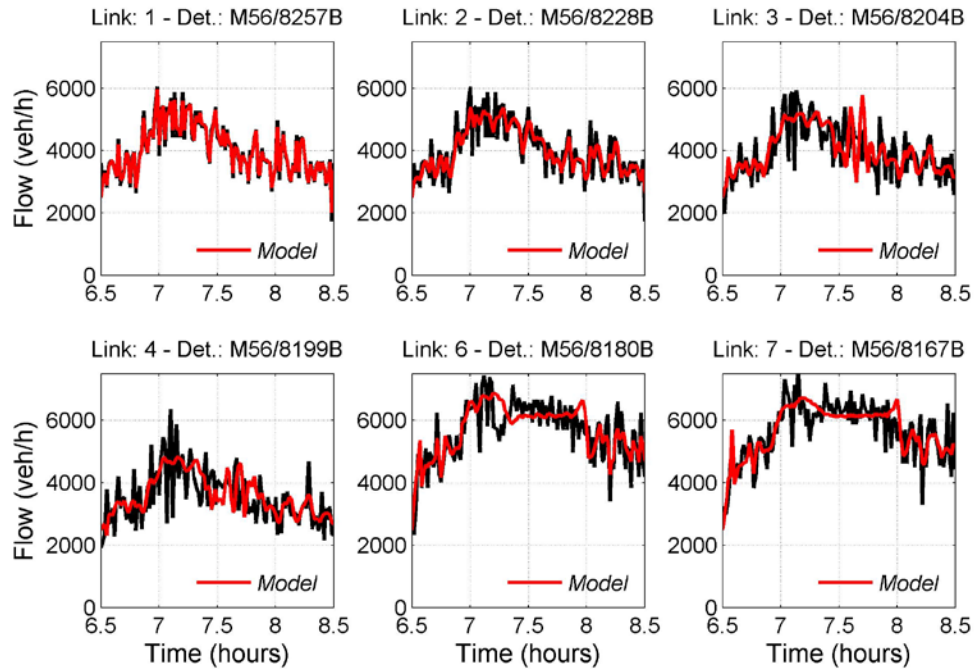

Figure 57 Time series of the real flow measurements and the second-order model METANET estimation of flow for 24/06/2014.